

Continuous Flavor Symmetries and the Stability of Asymmetric Dark Matter

Fady Bishara^{1,2,*} and Jure Zupan^{1,†}

¹*Department of Physics, University of Cincinnati, Cincinnati, Ohio 45221, USA*

²*Theoretical Physics Department, Fermilab, P.O. Box 500, Batavia, IL 60510*

Abstract

Generically, the asymmetric interactions in asymmetric dark matter (ADM) models lead to decaying DM. We show that, for ADM that carries nonzero baryon number, the continuous flavor symmetries that generate the flavor structure in the quark sector also imply a looser lower bound on the mass scale of the asymmetric mediators between the dark and visible sectors. The mediators for $B = 2$ ADM that can produce a signal in the future indirect dark matter searches can thus also be searched for at the LHC. For two examples of the mediator models, with either the MFV or Froggatt-Nielsen flavor breaking pattern, we derive the FCNC constraints and discuss the search strategies at the LHC.

* bisharfy AT ucmail.uc.edu

† zupanje AT ucmail.uc.edu

I. INTRODUCTION

Dark matter (DM) is stable on cosmological time-scales. A principal question about the nature of DM is what mechanism ensures its stability? Commonly this is assumed to be a result of an exact symmetry (for a concise review of proposed stabilization mechanisms see, e.g., [1]). One possibility is that the stability of DM is ensured by a gauge symmetry, mimicking the way QED gauge invariance ensures the stability of the electron in the standard model [2–4]. A more frequent choice is to introduce a Z_2 symmetry by hand. A prominent example is R -parity in the MSSM, which both stabilizes DM and ensures the stability of the proton [5–7]. An exact Z_2 symmetry can be generated dynamically, e.g., as a remnant of a spontaneously broken $U(1)$ gauge symmetry, such as $U(1)_{B-L}$ [8–10]. An attractive possibility is that Z_2 , and consequently the DM stability, is an accidental symmetry. Examples include minimal DM [11, 12], hidden vector DM [13], and weakly interacting stable pions [14].

In this paper we explore a possibility that the discrete Z_2 that ensures the stability of DM is *both accidental and approximate*. As a result DM is metastable with decay times potentially close to its present observational bound of $\tau \gtrsim 10^{26}$ s. We focus on a particular subset of asymmetric DM models [15] (for a recent review see [16]), where DM carries baryon number. Our working assumptions are

- Baryon number is a conserved quantum number (it could, for instance, be gauged at high scales).
- There is a sector that efficiently annihilates away the symmetric component. The exact form is not directly relevant for our discussion.
- The observed flavor structure in the quark sector is explained by flavor dynamics in the UV while DM is not charged under flavor.

The flavor dynamics fixes the flavor structure of dark sector couplings to the visible sector in the same way that it fixes the structure of the SM Yukawa interactions. This has two important consequences. First, the exchange of DM in the loops does not generate dangerously large Flavor Changing Neutral Currents (FCNCs). Secondly, and most importantly, a

flavor singlet DM is stable on cosmological timescales even for TeV scale mediators between the dark and visible sectors. In this case, the nature of DM stability can even be probed directly at the LHC.

The underlying flavor symmetry is crucial for the stability of DM. We will demonstrate this for two realizations of flavor physics: the Minimal Flavor Violation (MFV) hypothesis and for abelian horizontal symmetries in the case where DM carries baryon number 2. In this case the mediators leading to the decay of DM can be at $\mathcal{O}(100\text{GeV})$. In contrast, for completely anarchic flavor couplings where DM couples to all quark flavors with $\mathcal{O}(1)$ couplings, the indirect DM bounds would require the mediators to have masses in the $\mathcal{O}(10\text{TeV})$ range. The implications of continuous flavor symmetries for DM interactions have also been explored in [17–28]. Our analysis differs from these studies in that we are assuming that DM is a flavor singlet (as is the case in most models of DM). This, along with its small mass and conserved baryon number, also ensures that DM is metastable in our setup. The stability of symmetry-less DM in the context of discrete flavor groups has been discussed in [29] (for the potential relation of discrete flavor groups in the leptonic sector and the stability of DM, see also [30–32]). The decaying DM in the context of ADM models was explored in [33–36].

The paper is structured as follows. In Sec. II we review the relation between DM mass and relic abundance in asymmetric DM models. In Sec. III we give two examples of flavor breaking models at the level of Effective Field Theory (EFT) analysis that can lead to metastable asymmetric DM. In Sec. IV we derive the indirect detection bounds on the two EFT set-ups. In Sec. V we give two examples of mediators that would lead to the EFT set-ups discussed in Sec. IV. The relevant bounds on the mediator masses and couplings, including collider signatures, are derived in Sec. VI. Conclusions are given in Sec. VII, while appendices contain technical details.

II. DARK MATTER MASS IN ASYMMETRIC DARK MATTER MODELS

Asymmetric Dark Matter (ADM) models [15, 37–45] address the question of why the DM density, Ω_χ , and the baryon density in the universe, Ω_B , are so close to each other, $\Omega_\chi \simeq 5.3\Omega_B$ [46]. In the standard weakly interacting massive particle (WIMP) models of

DM this is to some extent pure coincidence. In this case DM is a thermal relic and

$$\left(\frac{\Omega_\chi}{0.265}\right)\left(\frac{h}{0.673}\right)^2 \sim \frac{3 \times 10^{-27} \text{ cm}^3 \text{ s}^{-1}}{\langle \sigma v \rangle}, \quad (1)$$

with $\langle \sigma v \rangle$ the thermally averaged DM annihilation cross section. The coincidence $\Omega_\chi \sim \Omega_B$ then arises due to a fortuitous size of the annihilation cross section for a weakly coupled weak scale DM – the WIMP miracle.

In contrast, in ADM models the observed DM is not a thermal relic. Its relic abundance reflects the asymmetry in DM, χ , and anti-DM, χ^\dagger , densities in the early universe. The χ and χ^\dagger annihilate away, and only the asymmetric component remains. The coincidence of Ω_χ and Ω_B is then due to the fact that the DM relic abundance has the same origin as the baryon asymmetry. The difference between Ω_χ and Ω_B is simply due to the fact that the DM particle is more massive than a proton by a factor of a few. More precisely, to explain the observed Ω_χ the DM's mass needs to be (see Appendix B)

$$m_\chi = N_0 m_p \frac{\Omega_\chi}{\Omega_B} \frac{1}{(B-L)_\chi}, \quad (2)$$

where m_p is the proton mass. Here $(B-L)_\chi$ is the $B-L$ charge of the χ field. The exact value of numerical prefactor $N_0 \simeq \mathcal{O}(1)$ depends on when the operators transferring the baryon asymmetry between the visible and the dark sector decouple. For decoupling temperature above electroweak phase transition, and assuming that there are only the SM fields in the visible sector, gives $N_0 = 1.255$ for DM that is a complex scalar or a Dirac fermion. In this case the required DM mass is

$$m_\chi = (6.2 \pm 0.4) \text{ GeV} \frac{1}{(B-L)_\chi}, \quad (3)$$

where the error reflects the errors on $\Omega_\chi = 0.265 \pm 0.011$ and $\Omega_B = 0.0499 \pm 0.0022$ [46, 47].

We thus have

$$m_\chi = \{6.2, 3.1, 2.1\} \text{ GeV}, \quad \text{for } (B-L)_\chi = \{1, 2, 3\}, \quad (4)$$

where we only quote the central values. Deviations from the above relations are possible if for instance the visible sector contains additional degrees of freedom beyond the SM. In that case, m_χ in (2) is a functions of $[(B-L)_{\text{NP}}^2]$, $[Y^2]_{\text{NP}}$, and $[Y(B-L)]_{\text{NP}}$, i.e., the $(B-L)^2$, Y^2 and

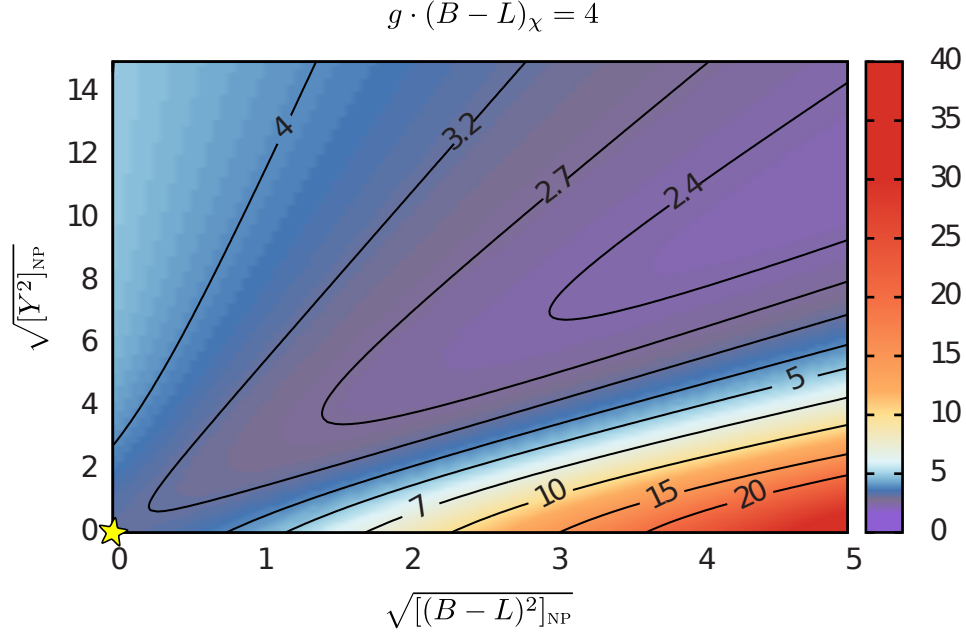


FIG. 1. Contours of the ADM mass m_χ (in GeV) required to obtain the correct DM relic density as a function of $[(B-L)^2]_{NP}$, $[Y^2]_{NP}$, i.e. the $(B-L)^2$, and Y^2 summed over effective d.o.f. in visible NP sector, while keeping $[Y(B-L)]_{NP} = \sqrt{[(B-L)^2]_{NP}[Y^2]_{NP}}$ and $g(B-L)_\chi = 4$. The visible sector with only the SM, Eq. (2), is denoted by a star.

$Y(B-L)$ summed over effective degrees of freedom in the visible NP sector, cf. Eq. (B17). The m_χ required to obtain the correct relic abundance is shown in Fig. 1. For illustration we set $[Y(B-L)]_{NP} = \sqrt{[(B-L)^2]_{NP}[Y^2]_{NP}}$ in the plot and assume that DM is a complex DM scalar with $(B-L)_\chi = 2$. We see that for $[(B-L)^2]_{NP} \sim [Y^2]_{NP} \sim [Y(B-L)]_{NP}$ the deviations from (4) are modest, of $\mathcal{O}(1)$. Further deviations from Eqs. (2), (4) are possible in more general frameworks such as ADM from leptogenesis [48] or dynamically induced mass mixing [49]. Henceforth, we will assume that m_χ is given by Eqs. (2), (4). Our results can be trivially adjusted if this is not the case.

The thermal history of the universe in ADM models has several distinct epochs. At high temperatures a $B-L$ asymmetry is generated, e.g., via GUT-like baryogenesis [15] or via leptogenesis [48]. The $B-L$ asymmetry is efficiently transferred between the visible and the DM sectors through asymmetric interactions. We do not require a discrete Z_n symmetry in

the dark sector so that unlike [15] the asymmetric interactions can involve just a single χ field. At low energies they have a schematic form,

$$\mathcal{O}_{\text{asymm.}} \sim \frac{C}{\Lambda^6} \chi(qq)^3, \quad (5)$$

taking $(B - L)_\chi = 2$ complex scalar DM as an example. Here, C is a flavor-dependent coefficient. The asymmetric interactions freeze out at temperature $T_f \sim \Lambda \gg m_\chi$, below which the $B - L$ asymmetries in the visible and dark sectors are separately conserved. If the flavor breaking is due to a spontaneously broken horizontal symmetry (see Sec. III B,) the freeze out temperature for the above dimension 10 operator in Eq. (5) is, using Naive Dimensional Analysis (NDA),

$$T_f \sim \left(1.66 \times \sqrt{g_*} (16\pi^2)^3 \frac{8\pi}{C^2} \frac{\Lambda^{12}}{M_{\text{Pl}}} \right)^{1/11} \simeq 450 \text{ GeV}. \quad (6)$$

In the numerical evaluation, we used the lower bound $\Lambda = \Lambda_* = 1.8 \text{ TeV}$ from indirect detection Eq. (22), taken the effective number of relativistic d.o.f. to be $g_* = 108.75$, corresponding to the SM with a complex scalar DM, and set $C = 1$ which is appropriate for the $\chi b \rightarrow bsc\bar{t}b$ transition dominance (with any permutation of the flavors). Note that T_f is above the electroweak phase transition temperature $T_{\text{ew}} \sim 170 \text{ GeV}$. It is also well below Λ so that the use of EFT is justified. If the mediator scale were too low, $\Lambda \lesssim 730 \text{ GeV}$ (or $\Lambda \lesssim 400 \text{ GeV}$ for MFV breaking), the asymmetric operator would not freeze out before electroweak phase transition started. Consequently, the DM quantum number would not be conserved and the DM density would be washed out. This places a lower bound on the asymmetric mediator masses to be above a few hundred GeV.

Finally, at temperatures below DM mass the bulk of the DM efficiently annihilates back to the visible sector through symmetric interactions leaving only the small asymmetric component. We have nothing new to say about this mechanism and refer the reader to a set of model building ideas already present in the literature [16, 50–52].

III. METASTABILITY AND FLAVOR BREAKING

We show next that the DM in ADM models can be stable on cosmological time-scales without invoking discrete Z_n symmetries. We assume that the SM quark flavor structure is explained by a continuous flavor group and that the DM carries nonzero baryon number. This is a crucial ingredient in the argument. Since DM is not charged under the flavor group, while the SM fields are, there are no interactions between DM and the SM in the limit that the flavor group is unbroken (all flavor singlet interactions are forbidden by baryon number conservation). All the interactions between DM and the visible sector thus have to be flavor breaking and this leads to a significant suppression of the DM decay time.

We show this explicitly for two examples of flavor breaking: i) the MFV ansatz, where all the flavor breaking is assumed to be due to the SM Yukawas, and ii) the spontaneously broken horizontal $U(1)$ symmetries. Integrating out the NP fields gives the effective DM decay Lagrangian

$$\mathcal{L} = \sum_i \frac{C_i}{\Lambda^{(D_i-4)}} \mathcal{O}_i. \quad (7)$$

The size of C_i is fixed by the assumed flavor generating mechanism. The sum runs over the different forms of the local operators

$$\mathcal{O}_i = \chi [u^c]^{n_u} [d^c]^{n_d} [q^*]^{n_q}, \quad (8)$$

where $(n_u + n_d + n_q) \bmod 3 = 0$ in order for DM to be a color singlet. Note that the DM needs to carry integer baryon number in order not to forbid all interactions with the visible sector. Here u^c , d^c are the electroweak singlets and q is the electroweak doublet left-handed quark fields in two component notation, see App. A. In the down-quark mass basis they are

$$u^c \rightarrow u_{\text{MASS}}^c, \quad d^c \rightarrow d_{\text{MASS}}^c, \quad q = \begin{pmatrix} u \\ d \end{pmatrix} \rightarrow \begin{pmatrix} V_{\text{CKM}} u_{\text{MASS}} \\ d_{\text{MASS}} \end{pmatrix}. \quad (9)$$

The SM Yukawa matrices are then

$$Y_D \rightarrow Y_D^{\text{diag}}, \quad Y_U \rightarrow V_{\text{CKM}} Y_U^{\text{diag}}, \quad (10)$$

with $Y_{D,U}^{\text{diag}}$ the diagonal Yukawa matrices.

As an example, let us consider fermionic $B = 1$ DM. Two distinct types of operators are allowed

$$\begin{aligned}\mathcal{O}_1^{(B=1)} &= (\chi u^c)(d^c d^c) \rightarrow (\chi u_{\text{MASS}}^c)(d_{\text{MASS}}^c d_{\text{MASS}}^c), \\ \mathcal{O}_2^{(B=1)} &= (\chi q_\rho^*)(d^c q_\sigma^*)\epsilon^{\rho\sigma} \rightarrow (\chi u_{\text{MASS}}^* V_{\text{CKM}})(d_{\text{MASS}}^c d_{\text{MASS}}^*),\end{aligned}\tag{11}$$

where ρ, σ are $SU(2)_L$ indices while the $SU(3)_C$ and flavor indices are implicit and we have chosen one possible Lorentz contraction denoted by the parentheses.

A. Minimal Flavor Violation

The MFV assumption is that also in the NP sector the flavor is broken only by the SM Yukawas $Y_{U,D}$ [53–57]. The MFV assumption can be most succinctly cast in the spurion language [54]. In the limit of vanishing quark masses the SM quark sector enjoys an enhanced flavor symmetry $G_F = SU(3)_Q \times SU(3)_U \times SU(3)_D$. The Yukawa interactions $u^e Y_U^\dagger q H$, $d^c Y_D^\dagger q H^c$ are formally invariant under G_F , if $Y_{U,D}$ are promoted to spurions, i.e. if they are assumed to transform under G_F as $Y_U \rightarrow Y'_U = U_Q Y_U U_U^\dagger$, $Y_D \rightarrow Y'_D = U_Q Y_D U_D^\dagger$. Here $U_{Q,U,D}$ are transformations from $SU(3)_{Q,U,D}$, respectively.

This means that also low energy operators (7) need to be formally G_F invariant. Keeping the minimal insertion of Yukawas the operators $\mathcal{O}_{1,2}$ in Eq. (11) for $B = 1$ DM are

$$\begin{aligned}\mathcal{O}_1^{(B=1)} &= (\chi u_\alpha^c Y_U^\dagger Y_D)_K (d_{N\beta}^c d_{M\gamma}^c) \epsilon^{KNM} \epsilon^{\alpha\beta\gamma} \\ &\rightarrow (\chi u_{\text{MASS}}^c Y_U^{\text{diag}\dagger} V_{\text{CKM}}^\dagger Y_D^{\text{diag}})_{K\alpha} ([d_{\text{MASS}}^c]_{N\beta} [d_{\text{MASS}}^c]_{M\gamma}) \epsilon^{KNM} \epsilon^{\alpha\beta\gamma}, \\ \mathcal{O}_2^{(B=1)} &= (\chi q_{K\alpha i}^* ([d_\beta^c Y_D^\dagger]_{N\gamma} q_{M\gamma j}^*)) \epsilon^{ij} \epsilon^{KNM} \epsilon^{\alpha\beta\gamma} \\ &\rightarrow (\chi u_{\text{MASS}}^* V_{\text{CKM}}^\dagger)_{K\alpha} ([d_{\text{MASS}}^c Y_D^{\text{diag}\dagger}]_{N\beta} [d_{\text{MASS}}^*]_{M\gamma}) \epsilon^{KNM} \epsilon^{\alpha\beta\gamma},\end{aligned}\tag{12}$$

where α, β, γ are the color indices, and K, N, M run over the quark generations.

The two operators lead to the $\chi \rightarrow bus$ decay at the partonic level which is the least suppressed kinematically allowed transition. For the operator \mathcal{O}_1 , this transition arises at 1-loop and requires two chirality flips, see Fig. 2. The decay amplitude scales as $\sim y_t y_b$ with an extra loop factor and a chirality flip suppression $\sim m_t \Lambda_{\text{QCD}} / m_W^2$. To be conservative, we count the chirality flip suppression due to the light u, d, s quarks as proportional to Λ_{QCD}

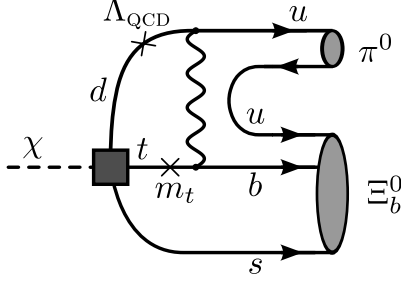


FIG. 2. Feynman diagram for the decay of DM with $B = 1$ assuming MFV. This amplitude leads to the partial decay width $\Gamma_\chi^{(1)}$ in Eq. (13).

and not to the much smaller quark masses. The operator \mathcal{O}_2 leads to the decay $\chi \rightarrow bus$ at tree level with the decay amplitude suppressed by $\sim y_b V_{ub}$. Once the quarks hadronize, the decays appear as $\chi \rightarrow \Xi_b \pi$, or $\chi \rightarrow \Lambda_b K$, with any number of pions. Using NDA to estimate the decay width gives (setting $V_{tb} \simeq V_{ud} \simeq 1$)

$$\begin{aligned} \Gamma_\chi^{(1)} &\sim \frac{(y_t y_b)^2}{8\pi} \left(\frac{m_\chi}{\Lambda}\right)^4 \left(\frac{1}{16\pi^2} \frac{m_t \Lambda_{\text{QCD}}}{m_W^2}\right)^2 \frac{m_\chi}{16\pi^2} = 6.6 \cdot 10^{-51} \text{GeV} \left(\frac{y_b}{0.024}\right)^2 \left(\frac{4.0 \cdot 10^6 \text{TeV}}{\Lambda}\right)^4, \\ \Gamma_\chi^{(2)} &\sim \frac{|y_b V_{ub}|^2}{8\pi} \left(\frac{m_\chi}{\Lambda}\right)^4 \frac{m_\chi}{16\pi^2} = 6.6 \cdot 10^{-51} \text{GeV} \left(\frac{y_b}{0.024}\right)^2 \left(\frac{4.3 \cdot 10^7 \text{TeV}}{\Lambda}\right)^4, \end{aligned} \quad (13)$$

for the case where \mathcal{O}_1 and \mathcal{O}_2 dominate the decay, respectively. The last $1/16\pi^2$ factor is due to three body final state and is required to obtain the correct estimate for the inclusive decay width as can be seen from the optical theorem and the use of OPE. In the numerics we use $m_t = 173 \text{ GeV}$, $m_\chi = 6.2 \text{ GeV}$, $|V_{ub}| = 0.00415$. The numerical prefactor $6.6 \cdot 10^{-51} \text{ GeV} = 1/(10^{26} s)$ is chosen to make contact with the bounds on the DM lifetime from indirect DM searches.

Note that MFV leads to two sources of suppression. First, there is the suppression of the Wilson coefficients due to Yukawa insertions, $y_b \sim 0.024$ for \mathcal{O}_1 and $y_b V_{ub} \sim 10^{-4}$ for \mathcal{O}_2 . In addition, there is a loop suppression for \mathcal{O}_1 where the decay has to proceed through an off-shell top quark. Without these additional suppressions the bounds from indirect DM detection would require about two orders larger NP scale, $\Lambda \gtrsim 4.3 \cdot 10^9 \text{ TeV}$.

The suppression factors are much larger for $B = 2$ DM, in which case DM is a scalar, and

the asymmetric operators start at dimension 10. We investigate in detail the operator

$$\begin{aligned}
\mathcal{O}_1^{(B=2)} &= \chi(d_{K\alpha}^c d_{N\beta}^c)([q^* Y_D]_{M\alpha'} q_{K'\beta'}^*)(q_{N'\gamma'}^* q_{M'\gamma}^*) \epsilon^{KNM} \epsilon^{K'N'M'} \epsilon^{\alpha\beta\gamma} \epsilon^{\alpha'\beta'\gamma'} \\
&\rightarrow \chi([d_{\text{MASS}}^c]_{K\alpha} [d_{\text{MASS}}^c]_{N\beta})([u_{\text{MASS}}^* V_{\text{CKM}}^\dagger Y_D^{\text{diag}}]_{M\alpha'} [d_{\text{MASS}}^*]_{K'\beta'}) \times \\
&\quad \times ([u_{\text{MASS}}^* V_{\text{CKM}}^\dagger]_{N'\gamma'} [d_{\text{MASS}}^*]_{M'\gamma}) \epsilon^{KNM} \epsilon^{K'N'M'} \epsilon^{\alpha\beta\gamma} \epsilon^{\alpha'\beta'\gamma'},
\end{aligned} \tag{14}$$

that gives the least suppressed decay amplitude. Above, we chose one of the possible color contractions, implicitly assumed contractions of weak indices within brackets, and only kept the weak contraction leading to the largest decay rate in the second line.

The correct relic abundance requires DM mass of $m_\chi = 3.1 \pm 0.2$ GeV, assuming the SM field content at the time of the decoupling of the asymmetric operators. We assume that $m_\chi < m_{\Lambda_c^+} + m_{\Sigma^-} = 3.48$ GeV, and thus below the threshold for the $\chi \rightarrow \Lambda_c^+ \Sigma^-$ decay, kinematically forbidding the $\chi \rightarrow udc dds$ partonic transition. The least suppressed partonic level transition is therefore $\chi \rightarrow uds uds$ resulting, after hadronization, in the decays $\chi \rightarrow \Lambda^0 \Lambda^0, \Sigma^- \Sigma^+, \Xi^- p, \Xi^0 n, \dots$. The NDA estimate of the χ decay width is then

$$\Gamma_\chi^{(1)} \sim \frac{|y_b V_{ub}^2|^2}{8\pi} \left(\frac{m_\chi}{\Lambda}\right)^{12} \frac{m_\chi}{(16\pi^2)^4} = 6.6 \cdot 10^{-51} \text{GeV} \left(\frac{y_b}{0.024}\right)^2 \left(\frac{0.63 \text{ TeV}}{\Lambda}\right)^{12}. \tag{15}$$

The MFV assumption results in the $y_b V_{ub}^2$ suppression of the Wilson coefficient. The $1/(16\pi^2)^4$ factor reflects the fact that, in the OPE, the leading contribution starts at 5 loops. The use of the OPE may be suspect for such low m_χ masses and one could expect $\mathcal{O}(1)$ corrections to the above estimate from additional soft gluon loops.

Indirect DM searches require the NP scale to be $\Lambda \gtrsim 0.49$ TeV. This corresponds to the bounds on the masses of the mediators between the dark and the visible sectors, $m_{\text{mediator}} \gtrsim 490$ GeV, $m_{\text{mediator}} \gtrsim 210$ GeV, and $m_{\text{mediator}} \gtrsim 90$ GeV, if the operator (14) arises at tree level, 1-loop, or 2-loop, respectively. The mediators can thus be searched for at the LHC as discussed in Sec. VIC. Note that the flavor suppression was essential to have such a low bound on the NP scale Λ . Without it, and taking the Wilson coefficient to be 1, the indirect bounds on the stability of DM would require $\Lambda \gtrsim 7.3$ TeV, implying that the mediators were most likely out of reach of the LHC.

ADM model			MFV			FN		
B	Dim.	m_χ [GeV]	decay	τ [s]	Λ [TeV]	decay	τ [s]	Λ [TeV]
1	6	6.2	$\chi \rightarrow bus$	10^{26}	4.0×10^6	$\chi \rightarrow bus$	10^{26}	8.1×10^8
2	10	3.1	$\chi \rightarrow udsuds$	10^{26}	0.63	$\chi \rightarrow udsuds$	10^{26}	2.5
3	15	2.1	forbidden	∞	–	forbidden	∞	–

TABLE I. Leading decay modes for the $B = 1, 2, 3$ ADM assuming MFV or FN flavor breaking. The dimensionality of the decaying operators are denoted in the 2nd column. With the suppression scales Λ given in the 6th and 9th column the ADM decay time is $\tau \simeq 10^{26}$ s. The $B = 3$ ADM decays to quarks are kinematically forbidden.

The bound on the NP scale Λ is quite sensitive to the actual value of m_χ . For larger values of m_χ , the χ can decay to top and bottom quarks reducing the loop and CKM suppression of the decay width. This is illustrated in Fig. 3, where the NP scale is fixed to $\Lambda_{\text{MFV}} = 1$ TeV and m_χ is varied. As the kinematic thresholds for the χ decays to c or b quarks are reached, this results in a change of several orders of magnitude in the predicted decay time.

B. Spontaneously Broken Horizontal Symmetries

The suppression we found above using the MFV ansatz is model dependent. To illustrate this point we turn to $U(1)$ Frogatt-Nielsen (FN) models of spontaneously broken horizontal symmetries [58]. The suppression of the Wilson coefficients in the effective Lagrangian (7) is then given by the horizontal charges of the quarks in the operators. For instance, for the two $B = 1$ DM operators in (7)

$$\begin{aligned}
\mathcal{O}_1^{(B=1)} &= (\chi d_K^c) (u_N^c d_M^c) \rightarrow (\chi [d_{\text{MASS}}^c]_K) ([u_{\text{MASS}}^c]_N [d_{\text{MASS}}^c]_M), \\
\mathcal{O}_2^{(B=1)} &= (\chi q_{Ki}^*) (d_N^c q_{Mj}^*) \epsilon^{ij} \rightarrow (\chi [u_{\text{MASS}}^*]_K) ([d_{\text{MASS}}^c]_N [d_{\text{MASS}}^*]_M),
\end{aligned}
\tag{16}$$

the Wilson coefficients are

$$C_1 \sim \lambda^{|H(d_K^c)+H(u_N^c)+H(d_M^c)|}, \quad C_2 \sim \lambda^{|-H(q_K)+H(d_N^c)-H(q_M)|}.
\tag{17}$$

Here $H(u_K^c), \dots$, with $H(q_K^*) = -H(q_K)$, are the horizontal $U(1)$ charges of the quarks, and $\lambda \sim 0.2$ is the expansion parameter. The dependence of the operators and Wilson coefficients

on the generational indices KNM is implicit as are color, weak, and Lorentz contractions in (16).

An example of a horizontal charge assignment that gives phenomenologically satisfactory quark masses and CKM matrix elements is [59],

$$H(q, d^c, u^c) \Rightarrow \begin{matrix} & 1 & 2 & 3 \\ q & \begin{pmatrix} 3 & 2 & 0 \\ 3 & 2 & 2 \\ 3 & 1 & 0 \end{pmatrix} \\ d^c & \\ u^c & \end{matrix}, \quad (18)$$

where the column labels $\{1, 2, 3\}$ correspond to the first, second, and third generations of quarks.

Since the heavier flavors carry smaller charges the DM preferentially decays into the heaviest accessible states. As in MFV the dominant decay is $\chi \rightarrow bus$, except that the $y_b V_{ub} \sim \lambda^5$ suppression gets replaced by a much more modest $\sim \lambda^{|-H(q_1)+H(s^c)-H(q_3)|} = \lambda$. This is the largest scaling allowed by FN charges. In concrete UV mediator models the suppression can, in fact, be much more severe as we will see explicitly in the next Section.

For $B = 2$ DM the least suppressed operator is

$$\begin{aligned} \mathcal{O}_1^{(B=2)} &= \chi(d_K^c d_N^c)(q_M^* q_{K'}^*)(q_{N'}^* q_{M'}^*) \\ &\rightarrow \chi([d_{\text{MASS}}^c]_K [d_{\text{MASS}}^c]_N)([u_{\text{MASS}}^*]_M [d_{\text{MASS}}^*]_{K'})([u_{\text{MASS}}^*]_{N'} [d_{\text{MASS}}^*]_{M'}), \end{aligned} \quad (19)$$

suppressing again the color and weak contractions. The corresponding Wilson coefficient is suppressed by

$$C_1 \sim \lambda^{|H(d_K^c)+H(d_N^c)-H(q_M)-H(q_{K'})-H(q_{N'})-H(q_{M'})|}. \quad (20)$$

At the partonic level, the dominant decay is $\chi \rightarrow ussuds$ with a Wilson coefficient that is of parametric size $\sim \lambda^{|H(d^c)+H(s^c)-2H(q_2)-2H(q_1)|} = \lambda^5$. Note that in MFV this process proceeded through 2 loops so that the suppression was much more severe, $\sim V_{ts} V_{ub}/(16\pi^2)^2 \sim \lambda^5/(16\pi^2)^2$ at the amplitude level. While the suppression in FN case is much less than in the MFV case, it is still nontrivial. It lowers the scale of NP allowed by indirect DM searches from $\Lambda \gtrsim 7.3$ TeV, in the case of no flavor structure, to $\Lambda \gtrsim 2.5$ TeV in the FN case. Taking the bound from DM indirect detection searches gives $\Lambda \gtrsim 1.9$ TeV. If the operator arises

at tree level, 1-loop or 2-loops, this corresponds to mediator masses, $m_{\text{mediator}} \gtrsim 1.9$ TeV, $m_{\text{mediator}} \gtrsim 830$ GeV, and $m_{\text{mediator}} \gtrsim 360$ GeV, respectively.

IV. INDIRECT DETECTION

The asymmetric operators discussed in the previous section lead to a decaying DM which can be potentially seen in indirect DM searches. In our models, the χ decays hadronically. The decay products thus contain a number of charged particles and photons. The flavor composition of the final state depends on the mass, m_χ , and also on the assumed flavor breaking pattern. In Section III we discussed in detail the case of 6.2 GeV $B = 1$ DM, which decays through $\chi \rightarrow bus$ and a 3.1 GeV $B = 2$ DM that decays through $\chi \rightarrow udsuds$. After hadronization these result in the decays $\chi \rightarrow \Xi_b^0 \pi^0$ and $\chi \rightarrow \Lambda^0 \Lambda^0$, respectively. The dominant decays for other DM masses, assuming the MFV or FN flavor breaking patterns, are given in Appendix C. The DM lifetime dependence on m_χ is shown in Fig. 3 after fixing the NP scale to be $\Lambda = 1(3)$ TeV for the MFV (FN) flavor breaking.

To guide the eye, we also show in Fig. 3 the following bounds from indirect DM searches. The green (orange) line shows the constraint on the DM decay time from FERMI-LAT [60] for $\chi \rightarrow b\bar{b}(\mu^+\mu^-)$ decays using the NFW profile. The dash-dotted light red line shows the results of an analysis [62] based on AMS-02 [61] and assuming $\chi \rightarrow \mu^+\mu^-$. The light blue line shows the result of an analysis [64] assuming $\chi \rightarrow \bar{\nu}\nu$ decay based on Super-Kamiokande [63] bounds. The purple line is an exclusion curve from [33] based on galactic and extragalactic gamma ray flux measurements by Fermi [65–67]. The authors in [33] consider $\chi \rightarrow uds$ and $\chi \rightarrow cbs$ decays as two extreme choices for the flavor structure of the final states. The derived bounds on χ lifetime differ by less than a factor of 2 such that the two bounds overlap on the scale of Fig. 3. The decays we consider fall between these two extreme choices with potentially weakened bounds in our cases above $m_\chi \gtrsim \mathcal{O}(10)$ GeV due to the increased multiplicity of final states. The bounds cross the expected χ decay times at $m_\chi \sim 5$ GeV for $\Lambda_{\text{MFV}} = 1$ TeV suppression scale in the case of MFV flavor breaking and at $m_\chi \sim 4$ GeV for $\Lambda_{\text{FN}} = 3$ TeV suppression scale in the case of FN flavor breaking.

For the 3.1 GeV $B = 2$ DM we thus find that, for the MFV case, the indirect detection

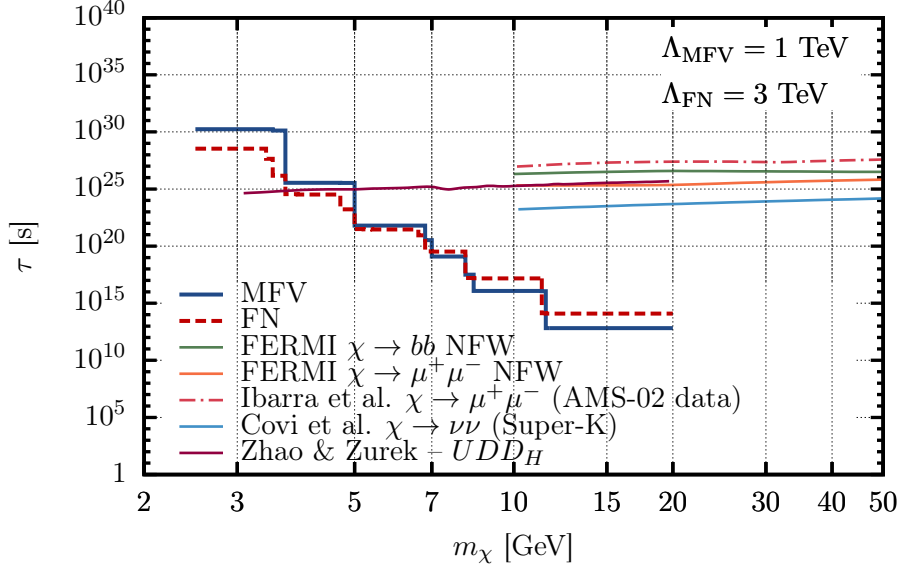


FIG. 3. The solid blue (red dashed) line denotes the $B = 2$ DM lifetime as a function of m_χ for the MFV (FN) case, fixing the NP scale to $\Lambda = 1(3)$ TeV. Assuming the dominance of one decay mode, the green (orange) line shows the constraint on the decay time from FERMI-LAT [60] for $b\bar{b}$ ($\mu^+\mu^-$) final states using the NFW profile. The dash-dotted red line shows the AMS-02 [61] constraint on $\chi \rightarrow \mu^+\mu^-$ decay time derived in [62], while the light blue line shows the Super-Kamiokande [63] constraint on the $\chi \rightarrow \nu\bar{\nu}$ decay time obtained in [64]. The purple line shows the upper limit on $\chi \rightarrow uds$ and $\chi \rightarrow cbs$ decay times (indistinguishable at the scale of the figure) obtained in [33].

requires

$$\Lambda_{\text{MFV}} \gtrsim 0.49 \text{ TeV}, \quad (21)$$

where the dominant operator is given in (14). For the FN case the bound is

$$\Lambda_{\text{FN}} \gtrsim 1.9 \text{ TeV}, \quad (22)$$

where the least suppressed operator is given in (19).

Field	$SU(3)_C$	$SU(2)_L$	$U(1)_Y$	G_F	$U(1)_{B-L}$
ϕ_L	$\bar{\mathbf{3}}$	$\mathbf{1}$	1/3	$(\mathbf{6}, \mathbf{1}, \mathbf{1})$	2/3
φ_L	$\mathbf{6}$	$\mathbf{1}$	1/3	$(\bar{\mathbf{3}}, \mathbf{1}, \mathbf{1})$	2/3
ϕ_R	$\bar{\mathbf{3}}$	$\mathbf{1}$	-2/3	$(\bar{\mathbf{3}}, \mathbf{1}, \mathbf{1})$	2/3

TABLE II. The gauge and global charge assignment for the three scalar mediators, ϕ_L , φ_L and ϕ_R , in the first UV completion toy model for which we assume the MFV flavor breaking pattern.

V. MEDIATOR MODELS

The EFT analysis of metastable ADM using asymmetric operators is an appropriate approach to derive the indirect DM detection signatures as we did in the previous section. However, for DM direct detection searches and the DM production at colliders, the dominant signals are due to either a single mediator exchange or from direct production of the mediators. To assess the reach of these DM searches, the UV completions to our models are therefore needed.

We introduce two toy model UV completions that can generate the dimension 10 effective operators; that is, the operator in Eq. (14) for the MFV case and the operator in Eq. (19) for the FN case. The EFT operators are generated when the \sim TeV mediators are integrated out. In our first model all the mediators are scalars, while in the second model there is also a fermionic mediator. The flavor structure in either of the two models could be of the MFV or of the FN type. For concreteness we fix the first model to have the MFV flavor breaking, and the second model to have the FN flavor breaking.

A. MFV model with scalar mediators

The SM is extended by the DM, χ , and three flavor multiplets of scalar mediators – a color anti-triplet ϕ_L and a color sextet φ_L , both with hypercharge 1/3, and a color sextet ϕ_R with hypercharge $-2/3$ (see Table II). They transform under the flavor group G_F as $(\mathbf{6}, \mathbf{1}, \mathbf{1})$, $(\bar{\mathbf{3}}, \mathbf{1}, \mathbf{1})$ and $(\bar{\mathbf{3}}, \mathbf{1}, \mathbf{1})$, respectively. The interaction Lagrangian between mediators and the

Field	$SU(3)_C$	$SU(2)_L$	$U(1)_Y$	$U(1)_{B-L}$
ϕ	$\bar{\mathbf{3}}$	$\mathbf{1}$	1/3	2/3
ψ	$\mathbf{1}$	$\mathbf{1}$	0	1

TABLE III. Gauge and $B - L$ charges of the mediators ϕ and ψ in the second UV completion toy model. We also assume the FN flavor breaking pattern.

SM is thus given by

$$\begin{aligned} \mathcal{L}_{\text{INT}} \supset & \frac{\kappa_1}{2} \bar{K}_I^{AB} [\phi_L]_\gamma^I (q_{A,\alpha}^* q_{B,\beta j}^*) \epsilon^{ij} \epsilon^{\alpha\beta\gamma} + \frac{\kappa_2}{2} \bar{K}_\lambda^{\alpha\beta} [\varphi_L]_A^\lambda (q_{B,\alpha i}^* q_{C,\beta j}^*) \epsilon^{ij} \epsilon^{ABC} \\ & + \frac{\kappa_3}{2} [Y_D]_X^A [\phi_R]_{A,\alpha} (d_{Y,\beta}^c d_{Z,\gamma}^c) \epsilon^{\alpha\beta\gamma} \epsilon^{XYZ} + \kappa_4 \bar{K}_I^{AB} \bar{K}_\lambda^{\alpha\beta} \chi^\dagger [\phi_L]_\alpha^I [\varphi_L]_A^\lambda [\phi_R]_{B,\beta} + h.c., \end{aligned} \quad (23)$$

where the flavor indices A, B, C belong to $SU(3)_Q$ and X, Y, Z to $SU(3)_D$. The QCD indices are $\alpha\beta\gamma$, while the weak isospin indices are denoted by i, j . The flavor index I and color index λ run from 1 to 6. The matrices of the Clebsch-Gordan coefficients, \bar{K}_I^{AB} and $\bar{K}_\lambda^{\alpha\beta}$, are the same as in [68] and satisfy the completeness relation $(\bar{K}_I^{AB})^* \bar{K}_I^{CD} = \frac{1}{2} (\delta_A^D \delta_B^C + \delta_A^C \delta_B^D)$, and similar for $\bar{K}_\lambda^{\alpha\beta}$. In the second line of (23), the down Yukawa insertions make the interaction term with right-handed down quarks formally invariant under G_F .

Integrating out the mediators $\phi_{L,R}, \varphi_L$, gives the χ decay operator (14), with the Wilson coefficient

$$\frac{\mathcal{C}_1}{\Lambda^6} = -\frac{1}{8} \frac{\kappa_1 \kappa_2 \kappa_3 \kappa_4}{m_{\phi_L}^2 m_{\varphi_L}^2 m_{\phi_R}^2}. \quad (24)$$

For $\kappa_1 = \kappa_2 = \kappa_3 = \kappa_4 = 1$ the bounds from indirect DM searches thus require $m_{\phi_L, \phi_R, \varphi_L} \gtrsim 450$ GeV, if all the mediator masses are the same. This should be appropriately rescaled if either κ_i have smaller values or if all masses are not the same. For instance, for $\kappa_i = 0.3$ the mass degenerate case of the mediators is bounded from below by $m_{\phi_L, \phi_R, \varphi_L} \gtrsim 200$ GeV. Since the mediators carry color charges, they can be searched for at the LHC as discussed in Section VIC below.

B. FN model with fermionic and scalar mediators

In the second model the SM is supplemented with DM scalar χ , a Dirac fermion ψ and a complex scalar ϕ with SM gauge assignments as in Table III. The relevant terms in the

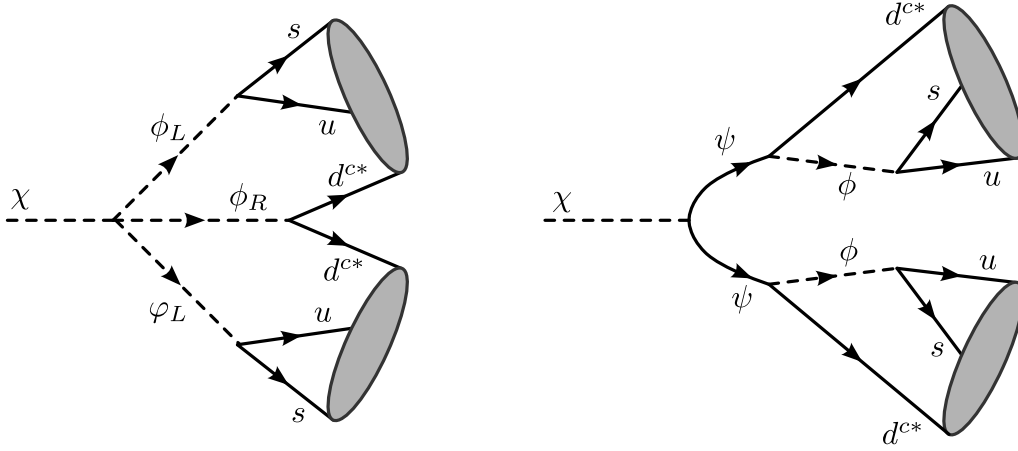


FIG. 4. The χ decay in the MFV mediator model through the off-shell scalar mediators $\phi_{L,R}, \varphi_L$ (left), and through the off-shell fermion ψ and scalar ϕ mediators in the FN model (right).

baryon number conserving interaction Lagrangian are

$$\mathcal{L}_{\text{INT}} \supset \frac{g_{q,AB}}{2} \phi_\gamma (q_{A,\alpha i}^{*j} q_{B,\beta j}^{*k}) \epsilon^{ij} \epsilon^{\alpha\beta\gamma} + g_{d,A} \phi^{*\alpha} (d_{A,\alpha}^c \psi) + \frac{g_\chi}{2} \chi (\psi^c \psi^c) + h.c. , \quad (25)$$

where, for the couplings g_q, g_d , we also denote the flavor dependence. If the flavor breaking is of the FN type and the mediators do not carry a horizontal charge, then

$$g_{q,AB} \sim g_q \lambda^{|H(q_A)+H(q_B)|}, \quad g_{d,A} \sim g_d \lambda^{|H(d_A)|}, \quad (26)$$

where $g_{q,d} \sim \mathcal{O}(1)$.

Integrating out the mediators generates the operator (19) with the Wilson coefficient

$$\frac{\mathcal{C}}{\Lambda^6} \simeq \frac{1}{8 m_\psi^2 m_\phi^4} g_\chi g_{q,M,K'} g_{q,N'M'} g_{d,K} g_{d,N} \sim \frac{1}{8 m_\psi^2 m_\phi^4} \lambda^{|H(d_K^c)|+|H(d_N^c)|+|H(q_M)+H(q_{K'})|+|H(q'_N)+H(q_{M'})|}. \quad (27)$$

Note that the flavor suppression here is parametrically different than in (20) which was obtained by assuming that the FN scale is close to the TeV scale and that the interactions of DM with the visible sector involve the FN fields. In the above model, however, the FN scale can be arbitrarily high and only fixes the flavor interactions between the mediator and the SM fields. Consequently, the leading decay is now $\chi \rightarrow ussuds$ where the suppression for the

amplitude is $\sim \lambda^{|H(d^c)|+|H(s^c)|+2|H(q_2)+H(q_1)|} \sim \lambda^{15}$, to be compared with the λ^4 suppression in the more conservative case considered in Section III B where the leading decay is $\chi \rightarrow udsuds$. The indirect detection bound (22) thus translates in our toy mediator model to $m_{\phi,\psi} \gtrsim 130$ GeV for mass degenerate ϕ and ψ . However, since the coupling to the third generation quarks is $\mathcal{O}(1)$, the scalar mediators should in fact be heavier than the top quark in order not to modify its total decay width.

The scaling (26) changes if the mediators carry nonzero horizontal charges. For instance, if the horizontal charge of ϕ is nonzero, $H(\phi) \neq 0$, one has $g_{q,AB} \sim \lambda^{|H(q_A)+H(q_B)-H(\phi)|}$, $g_{d,A} \sim \lambda^{|H(d_A)+H(\phi)|}$. In this case, the indirect detection bounds need to be appropriately rescaled. For $-2 \leq H(\phi) \leq 5$ the Wilson coefficient is still given by (27) and thus $m_{\phi,\psi} \gtrsim 130$ GeV from indirect bounds as before. For other values of $H(\phi)$, the bound becomes even weaker.

VI. EXPERIMENTAL SIGNATURES OF MEDIATORS

Now we turn to the experimental signatures of weak scale mediators, the flavor constraints, direct DM detection, and DM production at the LHC.

A. Flavor constraints

The two mediator models from Sec. V do not lead to tree level flavor changing neutral currents (FCNCs). These are first generated at 1-loop, see Fig. 5. For real couplings κ_i and $g_{q/d}$ in Eqs. (23), (25), the constraints from $K^0 - \bar{K}^0$, $D^0 - \bar{D}^0$ and $B_{(s)}^0 - \bar{B}_{(s)}^0$ mixing require the mediators masses to be generically above several hundred GeV, as we show below. For related analyses of flavor constraints on diquarks, see, e.g., [69, 70].

The $\Delta F = 2$ effective weak Hamiltonian is

$$\mathcal{H}_{\text{eff}}^{\Delta F=2} = \sum_i \mathcal{C}_i \mathcal{O}_i + \sum_i \tilde{\mathcal{C}}_i \tilde{\mathcal{O}}_i, \quad (28)$$

where $i = 1, \dots, 5$ runs over the dimension six operators (we use the notation in [71]). Integrating out the mediators and the W at the weak scale gives at leading order a nonzero

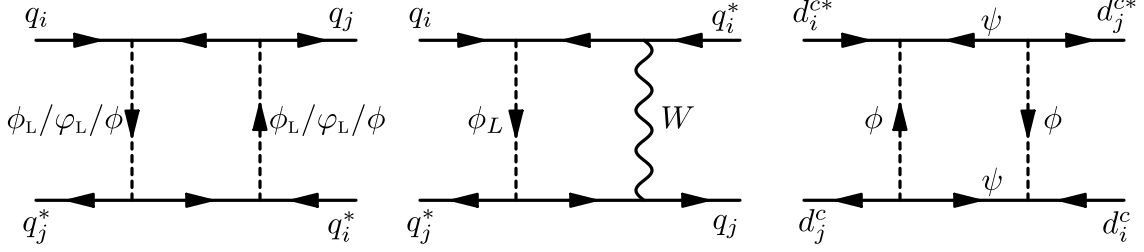


FIG. 5. Box diagrams contributing to the neutral meson mixing. In the MFV model, there is also a contribution with both ϕ_L and φ_L in the loop, while ϕ_R contributions are suppressed and can be ignored.

Wilson coefficient for the operator

$$\mathcal{O}_1 = (\bar{S}^\alpha \gamma_\mu P_L D^\alpha)(\bar{S}^\beta \gamma^\mu P_L D^\beta) = (s^{*\alpha} \bar{\sigma}^\mu d^\alpha) (s^{*\beta} \bar{\sigma}_\mu d^\beta), \quad (29)$$

in the case of the MFV model, and for both \mathcal{O}_1 and its parity conjugate operator

$$\tilde{\mathcal{O}}_1 = (\bar{S}^\alpha \gamma_\mu P_R D^\alpha)(\bar{S}^\beta \gamma^\mu P_R D^\beta) = (s^{c\alpha} \bar{\sigma}^\mu d^{c\alpha*}) (s^{c\beta} \bar{\sigma}_\mu d^{c\beta*}), \quad (30)$$

in the case of the FN model. Above we first give the operators in the 4-component notation and then also in the 2-component notation (for our notation see Appendix A).

In the matching there are two types of contributions, with only the mediators running in the loop, or with both the scalar mediator and the W boson running in the loop, see Fig. 5. For MFV model these give for the $K^0 - \bar{K}^0$, $D^0 - \bar{D}^0$, and $B_{(s)} - \bar{B}_{(s)}$ mixing

$$\mathcal{C}_{1K}^{\text{MFV}} = \frac{1}{64\pi^2 m_\phi^2} \left\{ (V_{cs} V_{cd}^*)^2 [(\kappa_1^4 + 3\kappa_2^4 - 2\kappa_1^2 \kappa_2^2) F(x_c) + 4g_w^2 \kappa_2^2 G(x_w, x_c)] + c \rightarrow t \right. \\ \left. - 2V_{cs} V_{cd}^* V_{ts} V_{td}^* [(\kappa_1^4 + 3\kappa_2^4 - 2\kappa_1^2 \kappa_2^2) F^F(x_c, x_t) + 4g_w^2 \kappa_2^2 G^F(x_w, x_c, x_t)] \right\}, \quad (31)$$

$$\mathcal{C}_{1D}^{\text{MFV}} = \frac{1}{64\pi^2 m_\phi^2} \left\{ (V_{us} V_{cs}^*)^2 [(\kappa_1^4 + 3\kappa_2^4 - 2\kappa_1^2 \kappa_2^2) F(x_s) + 4g_w^2 \kappa_2^2 G(x_w, x_s)] + s \rightarrow b \right. \\ \left. - 2V_{us} V_{cs}^* V_{ub} V_{cb}^* [(\kappa_1^4 + 3\kappa_2^4 - 2\kappa_1^2 \kappa_2^2) F^F(x_s, x_b) + 4g_w^2 \kappa_2^2 G^F(x_w, x_s, x_b)] \right\}, \quad (32)$$

$$\mathcal{C}_{1B_q}^{\text{MFV}} = \frac{1}{64\pi^2 m_\phi^2} (V_{tb} V_{tq}^*)^2 [(\kappa_1^4 + 3\kappa_2^4 - 2\kappa_1^2 \kappa_2^2) F(x_t) + 4g_w^2 \kappa_2^2 G(x_w, x_t)], \quad (33)$$

where $q = d, s$, $x_i = (m_i/m_\phi)^2$, and we have set $m_u = m_d = 0$ and taken for simplicity that the ϕ and φ are mass degenerate. The loop functions $F(x)$, $F^F(x_1, x_2)$, $G(x_1, x_2)$,

	MFV		FN	
	$\kappa_{1,2} <$	$m_{\phi_L, \varphi_L} >$	$g_{q,d} <$	$m_\phi >$
$K^0 - \bar{K}^0$	0.33	2.9 TeV	0.63	570 GeV
$B_d - \bar{B}_d$	1.3	710 GeV	0.54	1 TeV
$B_s - \bar{B}_s$	1.3	780 GeV	0.59	840 GeV
$D^0 - \bar{D}^0$	30	34 GeV	4.3	56 GeV

TABLE IV. The 95 % C.L. bounds on the MFV and FN mediator models from meson mixing. Taking $m_{\phi_L} = m_{\varphi_L} = m_\phi = 1\text{TeV}$ and $\kappa_1 = \kappa_2$ gives the upper bounds on the couplings in the 2nd column, and in 4th column for $g_q = g_d$. Taking in turn $\kappa_{1,2} = g_{q,d} = 1$ gives lower bounds on the mediator masses in 3rd and 5th columns. The mass of the fermion in the FN model is fixed to $m_\psi = 20$ GeV, see also Sec. VI C. The bounds are not very sensitive to m_ψ .

$G^F(x_1, x_2, x_3)$ are given in Appendix D. As in the SM also here the largest contribution to the $K^0 - \bar{K}^0$ mixing is due to the charm-charm loop, while for $B_q^0 - \bar{B}_q^0$ mixing the top loop dominates, as expected.

For the FN model the Wilson coefficients are given by

$$\mathcal{C}_{1K}^{\text{FN}} \sim \frac{\lambda^{10} g_q^4}{16\pi^2 m_\phi^2} \left[H(x_t) + 2\lambda^4 H^F(x_c, x_t) \right], \quad \tilde{\mathcal{C}}_{1K}^{\text{FN}} \sim \frac{\lambda^{10} g_d^4}{16\pi^2 m_\phi^2} H(x_\psi), \quad (34)$$

$$\mathcal{C}_{1B_d}^{\text{FN}} \sim \frac{\lambda^6 g_q^4}{16\pi^2 m_\phi^2} \left[H(x_t) + 2\lambda^4 H^F(x_c, x_t) \right], \quad \tilde{\mathcal{C}}_{1B_d}^{\text{FN}} \sim \frac{\lambda^{10} g_d^4}{16\pi^2 m_\phi^2} H(x_\psi), \quad (35)$$

$$\mathcal{C}_{1B_s}^{\text{FN}} \sim \frac{\lambda^4 g_q^4}{16\pi^2 m_\phi^2} \left[H(x_t) + 2\lambda^4 H^F(x_c, x_t) \right], \quad \tilde{\mathcal{C}}_{1B_s}^{\text{FN}} \sim \frac{\lambda^8 g_d^4}{16\pi^2 m_\phi^2} H(x_\psi), \quad (36)$$

and $\mathcal{C}_{1D}^{\text{FN}} = \mathcal{C}_{1K}^{\text{FN}}, \tilde{\mathcal{C}}_{1D}^{\text{FN}} = 0$. Above we have indicated the scaling of different contributions to the Wilson coefficient in terms of $\lambda = 0.2$, c.f., Sec. III B. In the numerics we use the equality sign. The loop functions $H(x)$ and $H^F(x_1, x_2)$ are given in Appendix D.

Note that the above Wilson coefficients contain $\log(m_i/m_\phi)$ that can become large for $m_\phi \gg m_i$. We do not attempt to resume these logarithms, which also means that we treat all the NP contributions as local. We expect that our numerical results can receive $\mathcal{O}(1)$ corrections due to neglected terms, which is within precision required for our analysis. We do include, though, the usual RGE effects due to the NLO QCD running of the effective

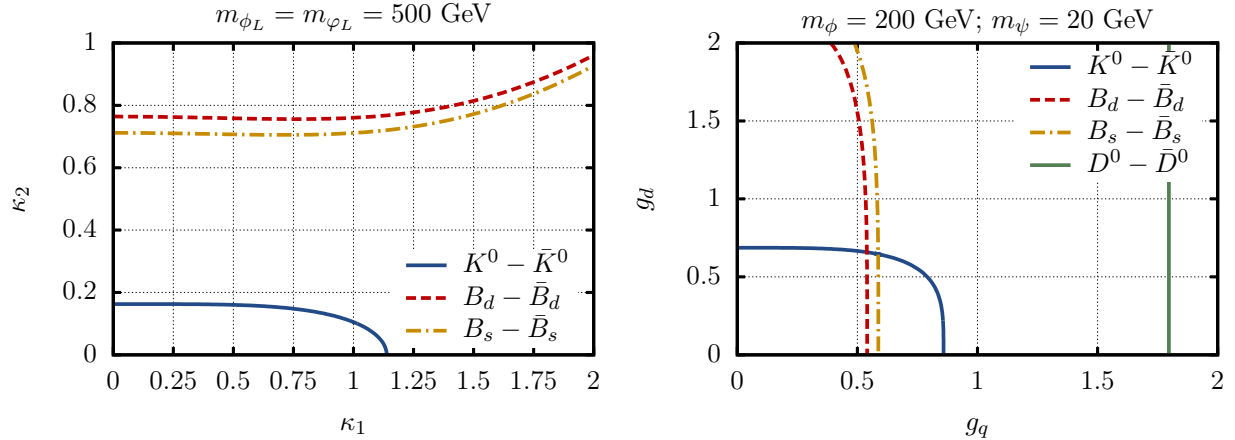


FIG. 6. Meson mixing constraints on the couplings $\kappa_{1,2}$ in the MFV mediator model (left) and $g_{q,d}$ in the FN model (right), taking $m_{\phi_L} = m_{\varphi_L} = 500 \text{ GeV}$ and $m_\phi = 200 \text{ GeV}$, $m_\psi = 20 \text{ GeV}$ respectively. The regions excluded are above and to the right of the curves.

weak Hamiltonian from the weak scale to the low energy. For constraints from $K^0 - \bar{K}^0$ and $B_{(s)} - \bar{B}_{(s)}$ mixing we use the recent results of a fit to the mixing parameters in [72]. The constraints from $D^- - \bar{D}^0$ mixing are obtained by that the NP contribution saturates Δm_D , so that in the equation $x_D = 2 |\langle \bar{D}^0 | \mathcal{H}_{\text{eff}}^{\Delta C=2} | D^0 \rangle| / \Gamma_D$, valid in the limit of no CP violation, we only include the NP contribution [71]. The resulting bounds on couplings and masses are shown in Table IV. In the case of MFV model the most severe bound comes from $K^0 - \bar{K}^0$ and is due to ϵ_K . Since we assume that all the κ_i in (23) are real, the NP contribution does carry a weak phase due to the $V_{ts}V_{td}^*$ CKM factors and does contribute to ϵ_K . In contrast for FN model the NP contribution to the mixing do not carry a weak phase, and thus to not have an effect on ϵ_K , and thus the bounds from $K^0 - \bar{K}^0$ mixing are much less severe.

In Fig. 6 we show the constraint on the couplings $\kappa_{1,2}$ in the MFV model, fixing $m_{\phi_L} = m_{\varphi_L} = 500 \text{ GeV}$ (left figure), and the constraints on $g_{q,d}$ in the FN model, fixing $m_\phi = 200 \text{ GeV}$, $m_\psi = 20 \text{ GeV}$ (right figure). Since in the case of MFV the largest contribution to $K^0 - \bar{K}^0$ is from the mediator- W loop, the ϵ_K bound places a stringent constraint on κ_2 . For $\kappa_2 \gg 1$, however, κ_1 can be $\mathcal{O}(1)$. Since the NP contributions to the meson mixing were assumed to be CP conserving in the case of the FN model, the couplings $g_{d,q} \sim \mathcal{O}(1)$ are allowed even for m_ϕ as low as 200 GeV.

B. Relic abundance and direct detection

We note in passing that the virtual exchanges of the mediators generate contact operators of the schematic form $\chi^\dagger\chi\bar{q}q$ that contribute to the $\chi\chi^\dagger$ annihilation cross section and to the cross section for DM scattering on nuclei. The symmetric couplings of DM and the mediators, of schematic form $\chi\chi^\dagger\phi\phi^\dagger$, do not suffice to create large enough annihilation cross sections that would annihilate away the symmetric component of DM relic abundance.

As an example consider the MFV model with scalar mediators, Eq. (23), and assume that the lightest mediator is ϕ_L . It can have a symmetric coupling to DM of the form

$$\mathcal{L} \supset \kappa' [\phi_L]_\gamma^I [\phi_L^\dagger]_\gamma^I \chi^\dagger \chi. \quad (37)$$

At 1-loop this generates a contact interaction $\chi^\dagger\partial_\mu\chi\bar{q}\gamma^\mu q$, which leads to annihilation cross section $\langle\sigma v\rangle \sim \mathcal{O}(10^{-28} \text{cm}^3/\text{s})(100\text{GeV}/m_{\phi_L})^4$ for $\mathcal{O}(1)$ couplings. This annihilation cross section is more than three orders of magnitude too small to obtain the observed relic density and satisfy CMB constraints for s -wave annihilation [50].

The symmetric component of DM thus needs to annihilate away through a different mechanism. An attractive possibility is that χ is charged under dark force which leads to large enough annihilation cross section [50–52]. The dark forces will then also lead to the dominant contribution to the direct detection cross section, for details see, e.g., [50].

C. Collider signatures

In both the MFV and FN flavor breaking scenarios the mediator models involve colored scalars. These can be searched for at the LHC through the gluon initiated pair production or through a single production. To estimate the LHC reach we use our two mediator models. The MFV mediator model, Eq. (23), contains three colored scalars that are either triplets or sextets of color and flavor group, see Table II. The FN model, Eq. (25), contains a colored scalar and a neutral fermion, see Table III.

Pair production of colored scalars is the dominant production mechanism of the mediators for the masses of interest, below $\mathcal{O}(\text{TeV})$. We illustrate this in Fig. 7 for the color triplet

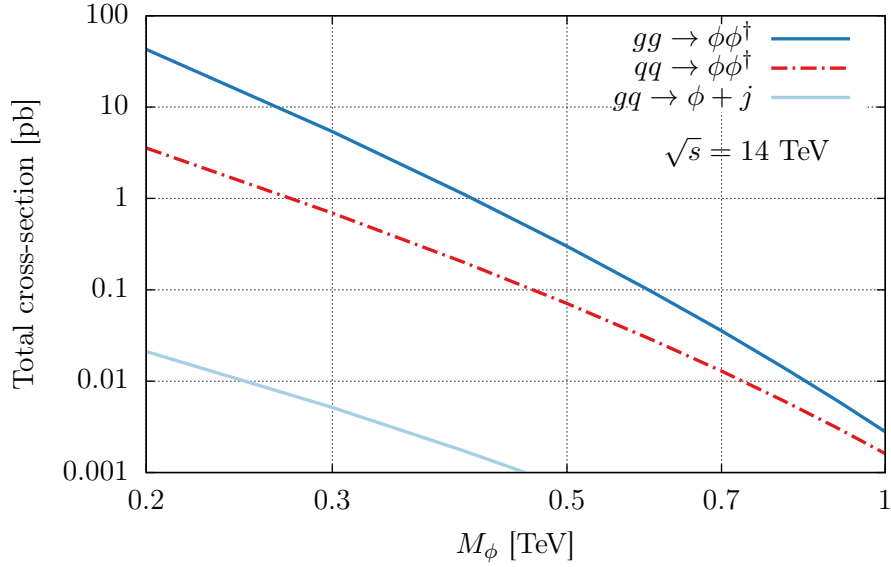


FIG. 7. The $gg \rightarrow \phi\phi^\dagger$ (solid blue), $qq \rightarrow \phi\phi^\dagger$ (dot-dashed red) and $qq \rightarrow \phi + j$ (solid light blue) contributions to the pair-production and single-production cross-section at the LHC with $\sqrt{s} = 14$ TeV as a function of a mass of a color triplet scalar ϕ , a mediator in the FN model.

ϕ in the FN model, where we compare the pair production cross section from gluon fusion and from quark-gluon fusion, and the single production of ϕ in association with a jet. Gluon fusion clearly dominates in the mass range of interest.

The signatures of pair produced colored scalars depend on their decay modes. In our two models they decay either directly to two SM quarks or, alternatively, first to two lighter scalars that then in turn decay to two jets each. In the FN model the decay $\phi \rightarrow j\psi$ is also possible. The flavor composition of the jets depends on the flavor quantum numbers of the scalar. For instance, the states in ϕ_L flavor multiplet can decay either predominantly through $\phi_L \rightarrow tb$, through $\phi_L \rightarrow bj$, or through $\phi_L \rightarrow jj$, depending on the flavor numbers of ϕ_L (and similarly for φ_L), see Eq. (23). The scalars in ϕ_R flavor multiplet, on the other hand, decay through $\phi_R \rightarrow bj$, or through $\phi_R \rightarrow jj$, again depending on the flavor index carried by the ϕ_R state. In the FN model one needs to require $m_\phi > m_t$ in order not to modify the total decay width of the top quark, see Sec. V. Then the dominant decay is either

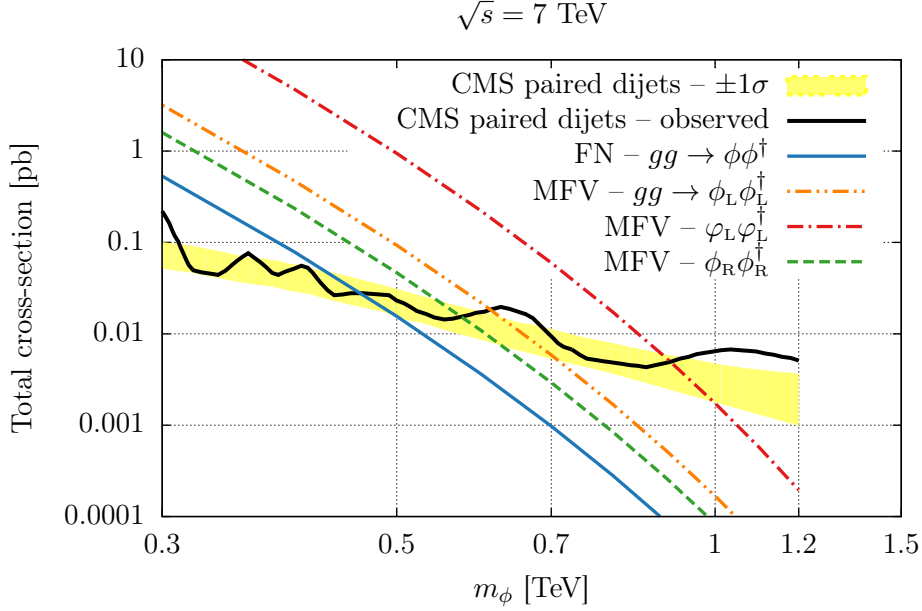


FIG. 8. Constraints on scalar mediator ϕ in the FN model, and ϕ_L , φ_L , ϕ_R in the MFV model, that follow from the CMS search for pair-produced dijet-resonances [73]. The state in the same flavor and color multiplet are taken to be mass-degenerate.

$\phi \rightarrow \bar{b}\psi$ or $\phi \rightarrow tb$, depending on the relative sizes of the two couplings, while the other decays are suppressed by additional powers of λ .

To get a rough estimate of the LHC sensitivity we treat all the decay modes as two-jet final states (this overestimates the reach slightly since for tj final state the real efficiency is expected to be lower). The strongest constraint on pair-production of the lightest scalar mediators is then the search for pair-produced dijet resonances from CMS at 7 TeV LHC with integrated luminosity of 5 fb^{-1} [73]. This places the bounds $m_\phi \gtrsim 470 \text{ GeV}$ in the case of FN model assuming that $\phi \rightarrow \bar{b}\psi$ decay is negligible, and $m_{\phi_L} \gtrsim 620 \text{ GeV}$, $m_{\varphi_L} \gtrsim 910 \text{ GeV}$, $m_{\phi_R} \gtrsim 580 \text{ GeV}$, in the case of MFV flavor breaking as shown in Fig. 8.

Note that when all three mediators are degenerate in mass, the color sextet scalar has the largest pair production cross section due to the large color factor.

For FN model a new experimental signature is obtained in the limit $g_d \gg \lambda^2 g_q$. Then the dominant decay of ϕ is $\phi \rightarrow \bar{b}\psi$. In order not to have fast decaying DM $m_\psi > m_\chi/$. Using

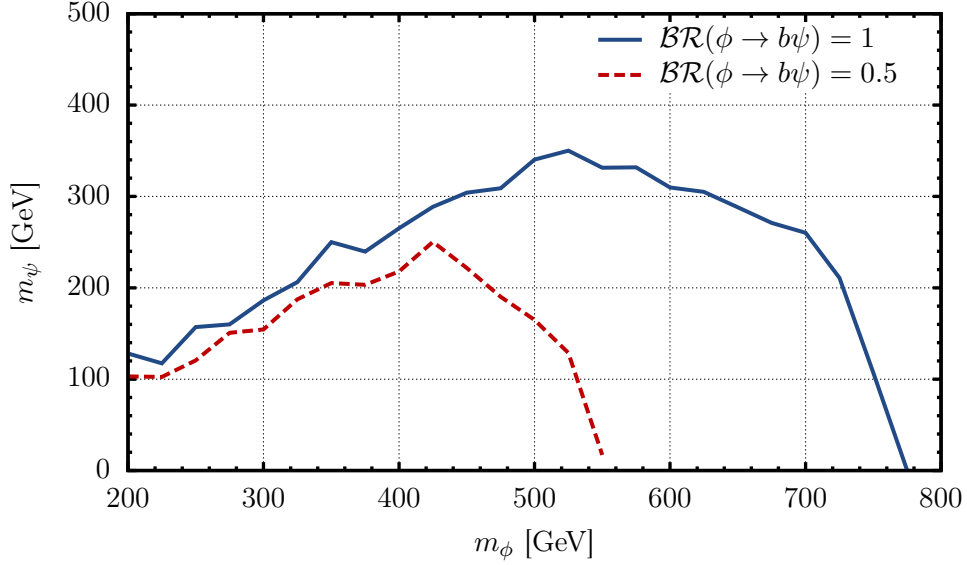


FIG. 9. The 95% exclusion limit on $\phi\phi^\dagger$ production in the FN model for the $b\bar{b}\psi\bar{\psi}$ final state, where ψ escapes the detector and sbottom search applies [74]. The solid blue (dashed red) line is for $\phi \rightarrow b\psi$ branching ratios of 50% and 100%.

NDA the ψ decay length is

$$c\tau(\psi \rightarrow bbc) \sim \left(g_q^2 g_d^2 \lambda^8 \frac{1}{8\pi} \frac{1}{16\pi^2} \frac{m_\psi^5}{m_\phi^4} \right)^{-1} \sim 30m \left(\frac{20 \text{ GeV}}{m_\psi} \right)^5 \left(\frac{m_\phi}{750 \text{ GeV}} \right)^4 \left(\frac{0.03}{g_q g_d} \right)^2. \quad (38)$$

For light enough m_ψ (or heavy enough m_ϕ), the fermion ψ does not decay in the detector and appears as \cancel{E}_T . The $pp \rightarrow \phi\phi^\dagger$ pair production then results in $2j + \cancel{E}_T$ or $2b + \cancel{E}_T$ final state, and is bounded from sbottom searches as shown in Fig. 9. The resulting bound is $m_\phi > 550(760)$ GeV for $m_\psi = 20$ GeV and $\mathcal{BR}(\phi \rightarrow \psi b) = 0.5(1.0)$. The choice $g_q g_d = 0.03$ in Eq. (38) gives $\mathcal{BR}(\phi \rightarrow b\psi) \approx \mathcal{BR}(\phi \rightarrow s\psi) = 0.33$. For the same input parameters the single production of ψ in association with b , t , or ϕ has a cross section $\sim 7 \cdot 10^{-2}$ fb while the pair production is dominated by the process $ss \rightarrow \psi\psi$ and has a negligible cross section of $\sim 4 \cdot 10^{-4}$ fb.

The single production of mediators, e.g., $ud \rightarrow \phi$, $ud \rightarrow \phi_L$, $ud \rightarrow \varphi_L$, $ds \rightarrow \phi_R$, is suppressed due to the small couplings of the mediators to the first and the second generation

quarks. Similarly, the single production from heavy quarks in the initial state suffers the PDF suppression.

For single top production, the MFV model gives the largest contribution with a cross-section of $\sigma(ud \rightarrow \phi_L \rightarrow tb)_{\text{MFV}} = 7.6 \times 10^{-6}$ pb for $m_{\phi_L} = 500$ GeV and $\sqrt{s} = 8$ TeV. This is well below the SM production cross section. Thus, the ATLAS and CMS combined measurement of the single top cross section at $\sqrt{s} = 8$ TeV, 85 ± 12 pb [75], does not impose any limits on the mediator model.

The production of DM χ can occur from the decay of heavier mediators. For instance, for $\kappa_4 \sim \kappa_3$ and ϕ_R heavy enough, the dominant decay mode of ϕ_3 is $\phi_3 \rightarrow \chi\varphi_L^\dagger\phi_L^\dagger$. Pair production $pp \rightarrow \phi_R\phi_R^\dagger$ would thus result in $8j + \cancel{E}_T$ signature, where paired dijets would reconstruct ϕ_L and φ_L mass peaks (depending on the flavor assignments some of the jets can be replaced by t or b jets).

VII. CONCLUSIONS

We showed that for asymmetric DM (ADM) models the stability of DM on cosmological time scales may be purely accidental. We do not require that the DM is charged under an ad-hoc conserved Z_n symmetry. Rather, we assume that such a discrete symmetry is explicitly broken by the mediator interactions that transfer the $B - L$ between the DM sector and the visible sector in the early universe. Such asymmetric interactions are necessary in all models of ADM though they may be made to obey a Z_4 symmetry (i.e. one can demand that they involve only the $\chi\chi \rightarrow \text{visible}$ or $\chi^\dagger\chi^\dagger \rightarrow \text{visible}$ transitions instead of $\chi \rightarrow \text{visible}$ transitions as is in our case).

At low energies, the DM then carries a conserved χ charge that is broken only by the higher dimensional operators obtained by integrating out the mediators. Such operators also lead to DM decays. In this paper we explored the role of continuous flavor symmetries for the properties of such decaying DM focusing on the case where DM that carries nonzero baryon number. For $B = 1$ DM, the direct detection bounds are evaded if the mediators are above $\sim 4 \cdot 10^9$ TeV assuming $\mathcal{O}(1)$ couplings. However, if quark flavor breaking is of the MFV type, the mediators can be lighter by around two orders of magnitude. For $B = 2$ DM,

the scale of mediators can be much lighter $\mathcal{O}(8\text{TeV})$ for $\mathcal{O}(1)$ couplings. This is then lowered by an order of magnitude if quark flavor breaking is of the MFV or Froggatt-Nielsen type. The mediators that would lead to indirect DM signals in the next generation of experiments can thus be, at the same time, searched for at the LHC.

We have explored this possibility by constructing two mediator models, one with assumed MFV and one with a FN flavor breaking pattern. The MFV mediator model (Eq. (23)) contains three colored scalars that are either triplets or sextets of the color and the flavor groups, see Table II. The FN model (Eq. (25)), on the other hand, contains one colored scalar and one neutral fermion, see Table III. These mediators generate FCNCs at 1-loop. While this leads to nontrivial constraints on their masses and couplings, the mediators can still be as light as a few $\times 100$ GeV with $\mathcal{O}(1)$ couplings. Since the mediators are charged under QCD, they can be singly or pair-produced at the LHC with large cross sections. This means that the searches at the LHC can lead to interesting constraints or discoveries. The signatures depend on how the mediators decay. In the FN model, for instance, the decay to heavy quarks, $\phi \rightarrow tb$, is favored. Modifying the paired dijet searches to the $pp \rightarrow \phi\phi \rightarrow tb\bar{t}\bar{b}$ signal could thus enhance the reach of the LHC in the search for these mediators. In the MFV model, on the other hand, paired light dijets, paired tb and paired bj are possible. Other signatures are discussed in Sec. VI C.

In conclusion, ADM can quite generically be metastable with a possibility of complementary signals in indirect detection and at the LHC.

Acknowledgements: J. Z. and F.B. are supported by the U.S. National Science Foundation under CAREER Grant PHY-1151392. F.B. is supported by the Fermilab Fellowship in Theoretical Physics. Fermilab is operated by Fermi Research Alliance, LLC, under Contract No. DE-AC02-07CH11359 with the United States Department of Energy. J.Z. is grateful to the Mainz Institute for Theoretical Physics (MITP) for its hospitality and its partial support during the completion of this work. J.Z. thanks the Aspen Center for Physics, supported by the NSF Grant #1066293, and the KITP, supported in part by the National Science Foundation under Grant No. NSF PHY11-25915, for their warm hospitality. F.B. thanks Prateek Agrawal, Roni Harnik, and Felix Yu for helpful discussions. Some of the cross-sections were computed using MadGraph5 [76] using a model file generated by FeynRules 2.0 [77].

Appendix A: Operators in four component notation

In the paper we are using a two-component notation, where the left-handed Weyl fermion fields $(q_i, u^c, d^c, l_i, e^c)$ have hypercharges $(+1/6, -2/3, +1/3, -1/2, +1)$ and $B - L$ charges $(1/3, -1/3, -1/3, -1, +1)$. The higgs doublet is denoted by H and has $Y = +1/2$, while $\tilde{H} = i\sigma_2 H^*$. The two Weyl spinors of the DM Dirac fermion are ψ and ψ^c with $B - L = -1$ and $+1$, respectively. Finally, ϕ is the complex scalar DM with $B - L = 2$. Capital letters denote four-component spinors following the notation in [78]. The DM Dirac fermion Ψ and its charge conjugate Ψ^C are

$$\Psi = \begin{pmatrix} \psi_\alpha \\ \psi^{c\dagger\dot{\alpha}} \end{pmatrix}, \quad \Psi^C = \begin{pmatrix} \psi_\alpha^c \\ \psi^{\dagger\dot{\alpha}} \end{pmatrix}, \quad (\text{A1})$$

while $\bar{\Psi} = (\psi^{c\alpha}, \psi_{\dot{\alpha}})$. Writing for the two-component spinors $q_1 = u_L, q_2 = d_L$ and $\ell_1 = \nu_L, \ell_2 = e_L$, suppressing generation indices, we introduce

$$U = \begin{pmatrix} u_{L\alpha} \\ u^{c\dagger\dot{\alpha}} \end{pmatrix}, \quad D = \begin{pmatrix} d_{L\alpha} \\ d^{c\dagger\dot{\alpha}} \end{pmatrix}, \quad E = \begin{pmatrix} e_{L\alpha} \\ e^{c\dagger\dot{\alpha}} \end{pmatrix}, \quad N = \begin{pmatrix} \nu_{L\alpha} \\ \nu^{c\dagger\dot{\alpha}} \end{pmatrix}, \quad (\text{A2})$$

where ν^c is the right-handed neutrino field introduced for completeness. If neutrino is Majorana, $\nu_L = \nu^c$. The weak doublets in the four-component notation are

$$Q_L = (U_L, D_L), \quad L_L = (N_L, E_L), \quad (\text{A3})$$

with $U_L \equiv P_L U$, etc, and similarly $U_R \equiv P_R U, D_R \equiv P_R D, \dots$. Some examples of the relevant asymmetric operators in the two- and four-component notations are given below.

$$\underline{\text{dim 6:}} \quad \mathcal{Q}_1^{(6)} = (q_i q^j)(d^{c*} \psi^{c*}) = (\overline{Q_{Li}^C} Q_L^i)(\overline{D^C} P_R \Psi), \quad (\text{A4})$$

$$\mathcal{Q}_2^{(6)} = (u^c d^c)(d^c \psi^c) = (\overline{U} P_L D^C)(\overline{D} P_L \Psi^C), \quad (\text{A5})$$

$$\underline{\text{dim 10:}} \quad \mathcal{Q}_1^{(10)} = \phi(d^c d^c)(q_i^* q^{i*})(q_j^* q^{j*}) = \phi(\overline{D} P_L D^C)(\overline{Q_{Li}} P_R Q_L^{Ci})(\overline{Q_{Li}} P_R Q_L^{Ci}). \quad (\text{A6})$$

Appendix B: Asymmetric DM relic density

Here we review the relations between the DM relic density and the DM mass in ADM models. We assume that the operator(s) transferring the $B - L$ asymmetry from the visible

to the dark sector decouple above electroweak phase transition, $T_C > T_{\text{ew}} \sim 170$ GeV [79], as is the case for our ADM models, see Sec. II. We first assume that the visible sector consists below T_C of only the SM fields (we will later relax this). The number density asymmetry for relativistic particles is

$$(n - \bar{n})_i = \frac{T^3}{6} \hat{g}_i \frac{\mu_i}{T}, \quad (\text{B1})$$

where $n(\bar{n})$ are the particle(anti-particle) number densities, μ_i is the chemical potential for species i , and $\hat{g}_i = g_i(g_i/2)$ for bosons (fermions) with g_i internal degrees of freedom so that $\hat{g}_i = 1$ for a Weyl fermion, while $\hat{g}_i = 2$ for a Dirac fermion or a complex scalar.

All the SM particles are in chemical equilibrium, so that the chemical potentials are proportional to the conserved quantum numbers [80]. Above the electroweak phase transition these are $B - L$, Y and $SU(2)_L$, while $B + L$ is broken by sphalerons. Thus (see also [81])

$$\mu_i = (T_3)_i c_3 + Y_i c_Y + (B - L)_i c_{B-L}, \quad (\text{B2})$$

where the c_i are constants that we determine from net weak isospin, hypercharge and $B - L$ densities. The net weak isospin charge density in the universe normalized to entropy density is

$$T_3 \propto \sum_i \hat{g}_i (T_3)_i \mu_i = \sum_i \hat{g}_i (T_3)_i^2 c_3 + 0 \cdot c_Y + 0 \cdot c_{B-L} = 0. \quad (\text{B3})$$

For the first equality we used that for each $SU(2)$ multiplet $\sum_i (T_3)_i = 0$, and in the second equality that the net T_3 charge is zero since $SU(2)_L$ is not explicitly broken. Thus $c_3 = 0$ and the $SU(2)_L$ charge of a particle does not contribute to its chemical potential.

Flavor mixing ensures that the chemical potentials for SM Weyl fermions from different generations are the same. Similarly, $SU(2)_L$ interactions ensure that $\mu_{u_L} = \mu_{d_L} \equiv \mu_Q$, and $\mu_{\ell_L} = \mu_\nu \equiv \mu_L$. We thus have

$$\begin{aligned} \mu_H &= \frac{1}{2} c_Y, & \mu_L &= -\frac{1}{2} c_Y - c_{B-L}, & \mu_E &= -c_Y - c_{B-L}, \\ \mu_Q &= \frac{1}{6} c_Y + \frac{1}{3} c_{B-L}, & \mu_U &= \frac{2}{3} c_Y + \frac{1}{3} c_{B-L}, & \mu_D &= -\frac{1}{3} c_Y + \frac{1}{3} c_{B-L}, \end{aligned} \quad (\text{B4})$$

while for the gauge bosons $\mu_G = \mu_W = \mu_B = 0$. The net hypercharge of the universe is thus

$$\begin{aligned} Y \propto \sum_i \hat{g}_i (Y)_i \mu_i &= \frac{1}{2} \cdot 2 \mu_H + N_f \left[-\frac{1}{2} 2 \mu_L - \mu_E + N_c \left(\frac{1}{6} \cdot 2 \mu_Q + \frac{2}{3} \mu_U - \frac{1}{3} \mu_D \right) \right] \\ &= 2 \mu_H + N_f (\mu_Q + 2 \mu_U - \mu_D - \mu_L - \mu_E) = 11 c_Y + 8 c_{B-L}, \end{aligned} \quad (\text{B5})$$

where $N_f = 3$ is the number of generations and N_c is the number of colors. Setting the net hypercharge density in the universe to zero, $Y = 0$, gives

$$c_Y = -\frac{8}{11}c_{B-L}. \quad (\text{B6})$$

The net $B - L$ number density in the visible sector (i.e. excluding the $B - L$ asymmetry carried by the χ fields in the dark sector) is then

$$B - L \propto N_f (-2\mu_L - \mu_E + 2\mu_Q + \mu_U + \mu_D) = \frac{79}{11}c_{B-L}. \quad (\text{B7})$$

There are two types of interactions between the dark and visible sector: the asymmetric interactions that involve a single χ field, and the symmetric interactions of the form $\chi^\dagger \chi$ times the SM fields. The symmetric operators keep the dark and the visible sectors in thermal equilibrium. The asymmetric interactions are suppressed, and decouple at temperatures well above the χ mass. At lower temperatures the χ number is thus effectively conserved. The chemical potential μ_χ is the same as it was before the decoupling. We thus have

$$\mu_\chi^i = (B - L)_\chi^i c_{B-L}, \quad (\text{B8})$$

where $(B - L)_\chi^i$ is the $B - L$ charge of the χ^i field. Here we allow for several χ^i fields in the dark sector and also define the weighted $B - L$ charge of the dark sector fields as

$$(B - L)_\chi^{\text{sum}} \equiv \sum_i \hat{g}_\chi^i (B - L)_\chi^i. \quad (\text{B9})$$

The net χ number density normalized to entropy density we denote by $\Delta\chi$ and is

$$\Delta\chi \propto \sum_i \hat{g}_\chi^i \mu_\chi^i = (B - L)_\chi^{\text{sum}} c_{B-L}. \quad (\text{B10})$$

Since $B - L$ and χ are conserved quantum numbers below the decoupling temperature, each of the number densities scales as R^{-3} as universe expands. The ratio

$$\frac{\Delta\chi}{B - L} = \frac{\Delta\chi}{B - L} \Big|_{\text{decoup.}} = \frac{11}{79} (B - L)_\chi^{\text{sum}}, \quad (\text{B11})$$

thus stays fixed.

Even if at the decoupling there are more χ_i dark sector states, we assume that DM is composed only from one state, χ . We therefore have for the ratio of baryon and dark matter energy densities

$$\frac{\Omega_B}{\Omega_\chi} = \frac{m_p}{m_\chi} \frac{B}{B-L} \frac{B-L}{\Delta\chi}. \quad (\text{B12})$$

The ratio of net B and $B-L$ numbers $B/(B-L) = 28/79 = 0.354$ just above the electroweak phase transition [80]. This remains essentially unchanged even if sphaleron and top mass effects are taken into account, in which case using results from [79, 82] one has $B/(B-L) = 0.349$ for both scalar and fermionic DM. Using $(B-L)/\Delta\chi = 79/(11(B-L)_\chi^{\text{sum}})$ from (B11) finally leads to

$$m_\chi = 2.509 m_p \frac{\Omega_\chi}{\Omega_B} \frac{1}{(B-L)_\chi^{\text{sum}}} = (12.5 \pm 0.8) \text{GeV} \frac{1}{(B-L)_\chi^{\text{sum}}}, \quad (\text{B13})$$

where in the last equality we used $\Omega_\chi = 0.265 \pm 0.011$ and $\Omega_B = 0.0499 \pm 0.0022$ [46]. Note that the error is dominated by the experimental determination of DM and baryon densities. For instance, the difference between $B/(B-L)$ determination with and without sphaleron effects leads to a smaller shift in m_χ than the above quoted error.

We turn next to the case of additional fields in the visible sector. An example would be that SM gets completed to the MSSM. The relation between $Y, B-L$ and the constants $c_{Y, B-L}$ can be written in the matrix form

$$\begin{aligned} \begin{pmatrix} Y \\ B-L \end{pmatrix} &= \frac{15}{4\pi^2 g_* T} \begin{pmatrix} \sum_i \hat{g}_i Y_i^2 & \sum_i \hat{g}_i Y_i (B-L)_i \\ \sum_i \hat{g}_i Y_i (B-L)_i & \sum_i \hat{g}_i (B-L)_i^2 \end{pmatrix} \cdot \begin{pmatrix} c_Y \\ c_{B-L} \end{pmatrix} \\ &= \frac{15}{4\pi^2 g_* T} \begin{pmatrix} 11 + [Y^2]_{\text{NP}} & 8 + [Y(B-L)]_{\text{NP}} \\ 8 + [Y(B-L)]_{\text{NP}} & 13 + [(B-L)^2]_{\text{NP}} \end{pmatrix} \cdot \begin{pmatrix} c_Y \\ c_{B-L} \end{pmatrix}. \end{aligned} \quad (\text{B14})$$

Here we defined

$$[Y^2]_{\text{NP}} = \sum_i \hat{g}_i Y_i^2, \quad [Y(B-L)]_{\text{NP}} = \sum_i \hat{g}_i Y_i (B-L)_i, \quad [(B-L)^2]_{\text{NP}} = \sum_i \hat{g}_i (B-L)_i^2, \quad (\text{B15})$$

where the sums run over the new states only. The solution for $B-L$ in terms of c_{B-L} is obtained by solving the above matrix equation setting $Y = 0$, from which

$$B-L = \frac{15 c_{B-L}}{4\pi^2 g_* T} \left(13 + [(B-L)^2]_{\text{NP}} - \frac{(8 + [Y(B-L)]_{\text{NP}})^2}{11 + [Y^2]_{\text{NP}}} \right). \quad (\text{B16})$$

The net χ charge is still given by Eq. (B11), while the ratio Ω_B/Ω_χ is given by (B12) with $(B-L)/\Delta\chi$ fixed at the decoupling temperature and $B/(B-L)$ at the electroweak phase transition. We thus have

$$m_\chi = m_p \frac{\Omega_\chi}{\Omega_B} \frac{B}{B-L} \left(13 + [(B-L)_{\text{NP}}]^2 - \frac{(8 + [Y(B-L)]_{\text{NP}})^2}{(11 + [Y^2]_{\text{NP}})^2} \right) \frac{1}{(B-L)_\chi^{\text{sum}}}, \quad (\text{B17})$$

where $B/(B-L) = 0.349$ and $(B-L)_\chi^{\text{sum}}$ given in (B9).

Appendix C: Calculation of the DM decay time

Here we give further details of the DM lifetime calculation in the MFV and FN models for $B = 2$ DM, Sec. III, while also varying the DM mass. The results are shown in Fig. 3. There are three different types of dimension 10 operators that can lead to DM decay, of schematic form $\chi(d^c d^c)(d^c d^c)(u^c u^c)$, $\chi(d^c d^c)(d^c u^c)(q^* q^*)$, and $\chi(q^* q^*)(q^* q^*)(d^c d^c)$. For the same NP suppression scale Λ the last type of operators gives the shortest lifetime. The dominant effective decay Lagrangian is thus, schematically,

$$\mathcal{L}_{\text{dec}}^{(B=2)} \supset \frac{\mathcal{C}}{\Lambda^6} \chi(q^* q^*)(q^* q^*)(d^c d^c), \quad (\text{C1})$$

where \mathcal{C} is a flavor-dependent Wilson coefficient, the brackets enclose Lorentz contracted pairs, and summation over different flavor, color and weak isospin contractions is understood.

In Sec. III we included the SM Yukawa insertions in the definition of the operators. To unify the notation we instead use in this appendix the convention that the Wilson coefficient \mathcal{C} encodes all the flavor suppressions. The effective decay Lagrangian is thus, going to the mass basis, and displaying the flavor indices only,

$$\mathcal{L}_{\text{dec.}}^{(B=2)} \supset \frac{\mathcal{C}^{\text{IJBCEF}}}{\Lambda^6} \chi u_1^* u_j^* d_B^* d_E^* d_C^c d_F^c, \quad (\text{C2})$$

where the flavor dependent Wilson coefficients are

$$\mathcal{C}_{(\text{MFV})}^{\text{IJBCEF}} \simeq [V_{\text{CKM}}]_{\text{IA}} [Y_d^{\text{diag}}]_{\text{B}} [V_{\text{CKM}}]_{\text{JD}} \varepsilon^{\text{ABC}} \varepsilon^{\text{DEF}}, \quad (\text{C3})$$

$$\mathcal{C}_{(\text{FN})}^{\text{IJBCEF}} \simeq \lambda^{|-H(q_1)-H(q_j)-H(q_B)-H(q_E)+H(d_C^c)+H(d_F^c)|}, \quad (\text{C4})$$

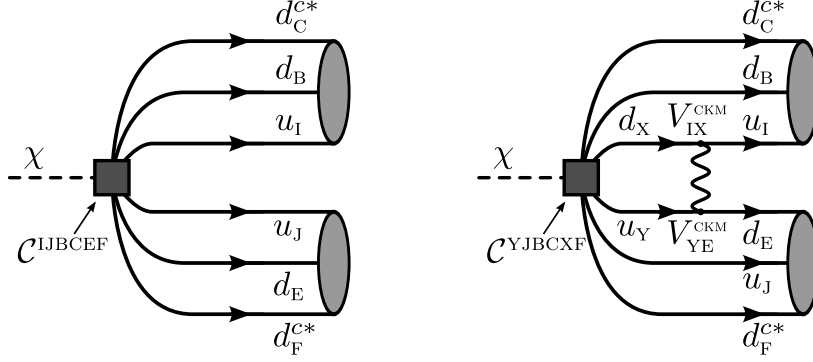


FIG. 10. Example Feynman diagrams for the decay of $B = 2$ DM. The diagram on the left shows the tree level decay whereas the one on the right shows the loop-induced decay.

The partial decay width for $\chi \rightarrow qq\bar{q}\bar{q}dd$ transition is then, using NDA,

$$\Gamma_\chi \simeq \frac{\mathcal{C}^2}{8\pi} \frac{1}{(16\pi^2)^4} \left(\frac{m_\chi}{\Lambda}\right)^{12} m_\chi. \quad (\text{C5})$$

The factor $1/(8\pi) \times 1/(16\pi^2)^4$ results from integrating over the 6-body phase space.

For the MFV flavor breaking case there are several subtleties when calculating the decay width. For instance, the Levi-Civita tensor contractions lead to vanishing operators for some of the color and Lorentz contractions. Another subtlety is that the tree decay may be strongly CKM suppressed so that the leading decay amplitude is the 1-loop one, see Fig. 10.

The decay width can thus be estimated as

$$\Gamma(\chi \rightarrow u_i u_j d_B d_E d_C^{c*} d_F^{c*}) \simeq \max \begin{cases} \frac{(C_{(\text{MFV})}^{\text{IJBCEF}})^2}{8\pi} \left(\frac{1}{16\pi^2}\right)^4 \left(\frac{m_\chi}{\Lambda}\right)^{12} m_\chi, \\ \left(\frac{1}{16\pi^2} [V_{\text{CKM}}]_{IX} [V_{\text{CKM}}]_{YE}\right)^2 \frac{(C_{(\text{MFV})}^{\text{YJBCXF}})^2}{8\pi} \left(\frac{1}{16\pi^2}\right)^4 \left(\frac{m_\chi}{\Lambda}\right)^{12} m_\chi. \end{cases} \quad (\text{C6})$$

where the first (second) line gives the NDA estimates for the tree level (1-loop) dominated decay width. The W emitted from the left-handed quark lines coming from the effective decay vertex gives the additional CKM factors in the second line.

An example where the leading decay amplitude is generated at 1-loop is the $B = 2$ ADM with $m_\chi = 3.3$ GeV, discussed in Sec. III. Decays into final states with one charm, bottom or top quark are kinematically forbidden. For instance, the lightest $B = 2$ final states with one valence charm quark are $\Lambda_c^+ + \Sigma^-$ and $n + \Sigma_c^0$. The first has the valence quark content

$\sim udc + dds$ and the rest mass $m_{\Lambda_c^+} + m_{\Sigma^-} = 3.48$ GeV, while the valence quark content of the second is $\sim udd + ddc$ and its rest mass $m_n + m_{\Sigma^0} = 3.4$ GeV. In contrast, the decays to Ξ^0 ($\sim uds$) or Λ^0 ($\sim uds$) baryons are allowed. Eq. (C6) gives

$$\Gamma_{\text{TREE}}^{\text{MFV}}(\chi \rightarrow \Lambda^0 \Lambda^0) \simeq (y_s V_{ub}^2)^2 \frac{1}{8\pi} \left(\frac{1}{16\pi^2}\right)^4 \left(\frac{m_\chi}{\Lambda}\right)^{12} m_\chi, \quad (\text{C7})$$

$$\Gamma_{\text{LOOP}}^{\text{MFV}}(\chi \rightarrow \Lambda^0 \Lambda^0) \simeq \left(\frac{y_b V_{ub} V_{ts}}{16\pi^2}\right)^2 \frac{1}{8\pi} \left(\frac{1}{16\pi^2}\right)^4 \left(\frac{m_\chi}{\Lambda}\right)^{12} m_\chi, \quad (\text{C8})$$

with the same estimate, within our precision, for the $\chi \rightarrow \Xi^0, \Xi^0$ or $\chi \rightarrow \Lambda^0, \Lambda^0$ decays. Note that in the 1-loop amplitude the partonic transition at the decay vertex, $\chi \rightarrow udb + tds$, carries no CKM suppression. Furthermore, the y_s Yukawa insertion in the tree level amplitude is replaced by y_b . The b and t quark lines then convert to u and s quark lines via W exchange, as shown in Fig. 10. The smaller CKM and Yukawa suppressions compensate the loop factor so that the 1-loop amplitude dominates, with the NDA estimate $\Gamma_{\text{LOOP}}^{\text{MFV}}/\Gamma_{\text{TREE}}^{\text{MFV}} \sim \mathcal{O}(10)$.

This procedure can be repeated for different DM masses, arriving at the dominant decay modes as a function of m_χ . The results are listed in Table V, where we give the kinematical thresholds (1st column) for a number of decay channels (4th column), along with the corresponding partonic transitions (3rd column) and the decay vertex transitions (2nd column). The latter two differ for the loop processes, cf. Fig. 10. The total decay width for given m_χ is then the sum of partial decay widths, Γ_i , (5th column) for the decay channels that are kinematically allowed. For convenience we also give the decay times, τ_i , (6th column) that correspond to individual partial decay widths. Note that in the calculation of the partial decay widths we neglect the phase space suppression, while the quoted Γ_i in Table V are obtained from the NDA estimates (C6) with m_χ at the kinematical threshold, and setting $\Lambda = 1\text{TeV}$.

In the case of FN flavor breaking the leading tree level and loop induced decay widths for $B = 2$, $m_\chi = 3.3$ GeV DM have the NDA estimates of

$$\Gamma_{\text{TREE}}^{\text{FN}}(\chi \rightarrow \Lambda^0 \Lambda^0) \simeq (\lambda^2)^2 \frac{1}{8\pi} \left(\frac{1}{16\pi^2}\right)^4 \left(\frac{m_\chi}{\Lambda}\right)^{12} m_\chi, \quad (\text{C9})$$

$$\Gamma_{\text{LOOP}}^{\text{FN}}(\chi \rightarrow \Lambda^0 \Lambda^0) \simeq \left(\frac{\lambda^4}{16\pi^2}\right)^2 \frac{1}{8\pi} \left(\frac{1}{16\pi^2}\right)^4 \left(\frac{m_\chi}{\Lambda}\right)^{12} m_\chi. \quad (\text{C10})$$

Thr. [GeV]	Decay vertex	Partonic	Final State	Γ_i [GeV]	τ_i [s]	Process
2.06	$\chi \rightarrow cudbsd$	$\chi \rightarrow udduds$	$n + \Lambda^0$	1.34×10^{-60}	4.91×10^{35}	Loop
2.23	$\chi \rightarrow wusdsd$	$\chi \rightarrow udsuds$	$\Lambda^0 + \Lambda^0$	3.74×10^{-55}	1.76×10^{30}	Tree
2.43	$\chi \rightarrow cusbsd$	$\chi \rightarrow udsuss$	$\Lambda^0 + \Xi^0$	4.25×10^{-57}	1.55×10^{32}	Loop
3.48	$\chi \rightarrow ccdssd$	$\chi \rightarrow udcdds$	$\Lambda_c^+ + \Sigma^-$	1.23×10^{-55}	5.33×10^{30}	Loop
3.61	$\chi \rightarrow ucsdsd$	$\chi \rightarrow udc dss$	$\Lambda_c^+ + \Xi^-$	1.87×10^{-50}	3.52×10^{25}	Tree
3.81	$\chi \rightarrow ccsdsd$	$\chi \rightarrow uds ssc$	$\Lambda^0 + \Omega_c^0$	1.42×10^{-52}	4.62×10^{27}	Loop
3.79	$\chi \rightarrow ccsdsd$	$\chi \rightarrow usc dss$	$\Xi_c^+ + \Xi^-$	1.33×10^{-52}	4.96×10^{27}	Loop
4.63	$\chi \rightarrow ccdbsd$	$\chi \rightarrow dcc dds$	$\Xi_{cc}^+ + \Sigma^-$	1.01×10^{-52}	6.51×10^{27}	Loop
4.93	$\chi \rightarrow ccsdsd$	$\chi \rightarrow ddc dsc$	$\Sigma_c^0 + \Xi_c^0$	1.04×10^{-46}	6.33×10^{21}	Tree
5.17	$\chi \rightarrow ccsbsd$	$\chi \rightarrow dsc ssc$	$\Xi_c^0 + \Omega_c^0$	4.14×10^{-52}	1.59×10^{27}	Loop
6.56	$\chi \rightarrow cud sbd$	$\chi \rightarrow udd udb$	$n + \Lambda_b^0$	7.25×10^{-54}	9.08×10^{28}	Loop
6.73	$\chi \rightarrow wud bsd$	$\chi \rightarrow udd usb$	$n + \Xi_b^0$	1.87×10^{-45}	3.53×10^{20}	Tree
6.94	$\chi \rightarrow wus bsd$	$\chi \rightarrow uss udb$	$\Xi^0 + \Lambda_b^0$	5.18×10^{-44}	1.27×10^{19}	Tree
7.10	$\chi \rightarrow cus dbs$	$\chi \rightarrow uss usb$	$\Xi^0 + \Xi_b^0$	3.49×10^{-52}	1.89×10^{27}	Loop
8.07	$\chi \rightarrow uc bdbd$	$\chi \rightarrow udb ddc$	$\Lambda_b^0 + \Sigma_c^0$	2.16×10^{-51}	3.05×10^{26}	Loop
8.09	$\chi \rightarrow uc bdsd$	$\chi \rightarrow udb dsc$	$\Lambda_b^0 + \Xi_c^0$	2.00×10^{-42}	3.30×10^{17}	Tree
8.31	$\chi \rightarrow uc bssd$	$\chi \rightarrow udb ssc$	$\Lambda_b^0 + \Omega_c^0$	5.33×10^{-41}	1.24×10^{16}	Tree
8.48	$\chi \rightarrow uc bsbs$	$\chi \rightarrow usb ssc$	$\Xi_b^0 + \Omega_c^0$	7.66×10^{-50}	8.59×10^{24}	Loop
11.24	$\chi \rightarrow wub dbd$	$\chi \rightarrow udb udb$	$\Lambda_b^0 + \Lambda_b^0$	2.24×10^{-42}	2.93×10^{17}	Tree
11.41	$\chi \rightarrow wub bsd$	$\chi \rightarrow udb usb$	$\Lambda_b^0 + \Xi_b^0$	9.86×10^{-38}	6.68×10^{12}	Tree
11.58	$\chi \rightarrow wub sbs$	$\chi \rightarrow usb usb$	$\Xi_b^0 + \Xi_b^0$	2.94×10^{-42}	2.24×10^{17}	Tree

TABLE V. Partial decay widths, Γ_i , and related decay times, $\tau_i = 1/\Gamma_i$, for representative decay channels above kinematical thresholds (1st column) assuming the MFV flavor breaking ansatz. The EFT scale is set to $\Lambda = 1$ TeV. The last column denotes whether the dominant amplitude is tree level or 1-loop, while the 2nd and the 3rd columns give the decay vertex transition and the partonic transition after the potential W exchange, respectively.

In this case the tree level decay dominates over the loop induced decay by four orders of magnitude. The dominance of the tree level decay amplitude over the 1-loop decay amplitude holds also, if the DM mass is varied. This can be traced to the following difference between the MFV and FN ansätze. In the MFV case the Levi-Civita tensors enforce that two quark flavors in the effective decay vertex need to be from the third generation. This can be changed either by using the V_{CKM} misalignment or through a loop transition. In FN flavor structure ansatz, on the other hand, the flavor indices need not be antisymmetric.

Appendix D: Loop functions in neutral meson mixing

Here we list the analytical form of the loop functions $F(x)$, $F^F(x_1, x_2)$, $G(x_1, x_2)$, $G^F(x_1, x_2, x_3)$ and $H(x)$, $H^F(x_1, x_2)$ that appear in the 1-loop expressions for the Wilson coefficients in the neutral meson mixing, Sec. VI A. The mediator loop functions with mass degenerate quarks in the loop are given by

$$F(x) = x H(x), \quad H(x) = \frac{1}{(1-x)^3} [1 - x^2 + 2x \log(x)], \quad (\text{D1})$$

while for two different quarks running in the loop they are

$$F^F(x_i, x_j) = \frac{x_i x_j}{(1-x_i)(1-x_j)} + \left[\frac{x_i x_j \log(x_i)}{(1-x_i)^2(x_i-x_j)} + x_i \leftrightarrow x_j \right], \quad (\text{D2})$$

$$H^F(x_i, x_j) = \frac{1}{(1-x_i)(1-x_j)} + \left[\frac{x_i^2 \log(x_i)}{(1-x_i)^2(x_i-x_j)} + x_i \leftrightarrow x_j \right]. \quad (\text{D3})$$

The loop functions for the mediator- W loops are

$$G(x_w, x) = \frac{x}{x_w} \left[\frac{x_w + x}{(x-1)(x-x_w)} - \frac{x(2xx_w - x_w^2 - 2x_w + x^2) \log(x)}{(x-1)^2(x-x_w)^2} + \frac{2xx_w \log(x_w)}{(x-x_w)^2(x_w-1)} \right], \quad (\text{D4})$$

$$G^F(x_w, x_i, x_j) = \frac{x_i x_j}{x_w} \left[\left\{ \frac{(x_i + x_w) \log(x_i)}{(1-x_i)(x_i-x_j)(x_w-x_i)} + x_i \leftrightarrow x_j \right\} - \frac{2x_w \log(x_w)}{(1-x_w)(x_w-x_i)(x_w-x_j)} \right]. \quad (\text{D5})$$

-
- [1] T. Hambye, PoS **IDM2010**, 098 (2011), arXiv:1012.4587 [hep-ph].
- [2] L. Ackerman, M. R. Buckley, S. M. Carroll, and M. Kamionkowski, Phys.Rev. **D79**, 023519 (2009), arXiv:0810.5126 [hep-ph].
- [3] J. L. Feng, H. Tu, and H.-B. Yu, JCAP **0810**, 043 (2008), arXiv:0808.2318 [hep-ph].
- [4] J. L. Feng, M. Kaplinghat, H. Tu, and H.-B. Yu, JCAP **0907**, 004 (2009), arXiv:0905.3039 [hep-ph].
- [5] G. R. Farrar and P. Fayet, Phys.Lett. **B76**, 575 (1978).
- [6] S. Dimopoulos, S. Raby, and F. Wilczek, Phys.Lett. **B112**, 133 (1982).
- [7] G. R. Farrar and S. Weinberg, Phys.Rev. **D27**, 2732 (1983).
- [8] M. Kadastik, K. Kannike, and M. Raidal, Phys.Rev. **D81**, 015002 (2010), arXiv:0903.2475 [hep-ph].
- [9] M. Kadastik, K. Kannike, and M. Raidal, Phys.Rev. **D80**, 085020 (2009), arXiv:0907.1894 [hep-ph].
- [10] M. Frigerio and T. Hambye, Phys.Rev. **D81**, 075002 (2010), arXiv:0912.1545 [hep-ph].
- [11] M. Cirelli and A. Strumia, New J.Phys. **11**, 105005 (2009), arXiv:0903.3381 [hep-ph].
- [12] M. Cirelli, N. Fornengo, and A. Strumia, Nucl.Phys. **B753**, 178 (2006), arXiv:hep-ph/0512090 [hep-ph].
- [13] T. Hambye, JHEP **0901**, 028 (2009), arXiv:0811.0172 [hep-ph].
- [14] Y. Bai and R. J. Hill, Phys.Rev. **D82**, 111701 (2010), arXiv:1005.0008 [hep-ph].
- [15] D. E. Kaplan, M. A. Luty, and K. M. Zurek, Phys.Rev. **D79**, 115016 (2009), arXiv:0901.4117 [hep-ph].
- [16] K. M. Zurek, Phys.Rept. **537**, 91 (2014), arXiv:1308.0338 [hep-ph].
- [17] B. Batell, J. Pradler, and M. Spannowsky, JHEP **1108**, 038 (2011), arXiv:1105.1781 [hep-ph].
- [18] J. Kile and A. Soni, Phys.Rev. **D84**, 035016 (2011), arXiv:1104.5239 [hep-ph].
- [19] P. Agrawal, S. Blanchet, Z. Chacko, and C. Kilic, Phys.Rev. **D86**, 055002 (2012), arXiv:1109.3516 [hep-ph].

- [20] H. Davoudiasl, D. E. Morrissey, K. Sigurdson, and S. Tulin, *Phys.Rev.* **D84**, 096008 (2011), arXiv:1106.4320 [hep-ph].
- [21] L. Lopez-Honorez and L. Merlo, *Phys.Lett.* **B722**, 135 (2013), arXiv:1303.1087 [hep-ph].
- [22] P. Agrawal, M. Blanke, and K. Gemmler, (2014), arXiv:1405.6709 [hep-ph].
- [23] B. Batell, T. Lin, and L.-T. Wang, *JHEP* **1401**, 075 (2014), arXiv:1309.4462 [hep-ph].
- [24] P. Agrawal, B. Batell, D. Hooper, and T. Lin, (2014), arXiv:1404.1373 [hep-ph].
- [25] U. Haisch, A. Hibbs, and E. Re, *Phys.Rev.* **D89**, 034009 (2014), arXiv:1311.7131 [hep-ph].
- [26] J. F. Kamenik and J. Zupan, *Phys.Rev.* **D84**, 111502 (2011), arXiv:1107.0623 [hep-ph].
- [27] P. Agrawal, S. Blanchet, Z. Chacko, and C. Kilic, *Phys.Rev.* **D86**, 055002 (2012), arXiv:1109.3516 [hep-ph].
- [28] A. Merle and V. Niro, *JCAP* **1107**, 023 (2011), arXiv:1105.5136 [hep-ph].
- [29] Y. Kajiyama, K. Kannike, and M. Raidal, *Phys.Rev.* **D85**, 033008 (2012), arXiv:1111.1270 [hep-ph].
- [30] M. Lattanzi, R. A. Lineros, and M. Taoso, (2014), arXiv:1406.0004 [hep-ph].
- [31] M. Hirsch, S. Morisi, E. Peinado, and J. Valle, *Phys.Rev.* **D82**, 116003 (2010), arXiv:1007.0871 [hep-ph].
- [32] M. Boucenna, S. Morisi, E. Peinado, Y. Shimizu, and J. Valle, *Phys.Rev.* **D86**, 073008 (2012), arXiv:1204.4733 [hep-ph].
- [33] Y. Zhao and K. M. Zurek, *JHEP* **1407**, 017 (2014), arXiv:1401.7664 [hep-ph].
- [34] L. Feng and Z. Kang, *JCAP* **1310**, 008 (2013), arXiv:1304.7492 [hep-ph].
- [35] I. Masina, P. Panci, and F. Sannino, *JCAP* **1212**, 002 (2012), arXiv:1205.5918 [astro-ph.CO].
- [36] I. Masina and F. Sannino, *JCAP* **1109**, 021 (2011), arXiv:1106.3353 [hep-ph].
- [37] G. R. Farrar and G. Zaharijas, *Phys.Rev.Lett.* **96**, 041302 (2006), arXiv:hep-ph/0510079 [hep-ph].
- [38] R. Kitano and I. Low, *Phys.Rev.* **D71**, 023510 (2005), arXiv:hep-ph/0411133 [hep-ph].
- [39] R. Kitano, H. Murayama, and M. Ratz, *Phys.Lett.* **B669**, 145 (2008), arXiv:0807.4313 [hep-ph].
- [40] M. Fujii and T. Yanagida, *Phys.Lett.* **B542**, 80 (2002), arXiv:hep-ph/0206066 [hep-ph].
- [41] D. B. Kaplan, *Phys.Rev.Lett.* **68**, 741 (1992).

- [42] S. Nussinov, Phys.Lett. **B165**, 55 (1985).
- [43] S. M. Barr, Phys.Rev. **D44**, 3062 (1991).
- [44] S. M. Barr, R. S. Chivukula, and E. Farhi, Phys.Lett. **B241**, 387 (1990).
- [45] S. B. Gudnason, C. Kouvaris, and F. Sannino, Phys.Rev. **D73**, 115003 (2006), arXiv:hep-ph/0603014 [hep-ph].
- [46] J. Beringer *et al.* (Particle Data Group), Phys.Rev. **D86**, 010001 (2012).
- [47] P. Ade *et al.* (Planck Collaboration), (2013), arXiv:1303.5076 [astro-ph.CO].
- [48] A. Falkowski, J. T. Ruderman, and T. Volansky, JHEP **1105**, 106 (2011), arXiv:1101.4936 [hep-ph].
- [49] Y. Cui, L. Randall, and B. Shuve, JHEP **1108**, 073 (2011), arXiv:1106.4834 [hep-ph].
- [50] T. Lin, H.-B. Yu, and K. M. Zurek, Phys.Rev. **D85**, 063503 (2012), arXiv:1111.0293 [hep-ph].
- [51] T. Cohen, D. J. Phalen, A. Pierce, and K. M. Zurek, Phys.Rev. **D82**, 056001 (2010), arXiv:1005.1655 [hep-ph].
- [52] M. Blennow, E. Fernandez-Martinez, O. Mena, J. Redondo, and P. Serra, JCAP **1207**, 022 (2012), arXiv:1203.5803 [hep-ph].
- [53] R. S. Chivukula and H. Georgi, Phys.Lett. **B188**, 99 (1987).
- [54] G. D'Ambrosio, G. Giudice, G. Isidori, and A. Strumia, Nucl.Phys. **B645**, 155 (2002), arXiv:hep-ph/0207036 [hep-ph].
- [55] L. Hall and L. Randall, Phys.Rev.Lett. **65**, 2939 (1990).
- [56] A. J. Buras, Acta Phys.Polon. **B34**, 5615 (2003), arXiv:hep-ph/0310208 [hep-ph].
- [57] A. Buras, P. Gambino, M. Gorbahn, S. Jager, and L. Silvestrini, Phys.Lett. **B500**, 161 (2001), arXiv:hep-ph/0007085 [hep-ph].
- [58] C. Froggatt and H. B. Nielsen, Nucl.Phys. **B147**, 277 (1979).
- [59] M. Leurer, Y. Nir, and N. Seiberg, Nucl.Phys. **B420**, 468 (1994), arXiv:hep-ph/9310320 [hep-ph].
- [60] M. Ackermann *et al.* (LAT collaboration), Astrophys.J. **761**, 91 (2012), arXiv:1205.6474 [astro-ph.CO].
- [61] M. Aguilar *et al.* (AMS Collaboration), Phys.Rev.Lett. **110**, 141102 (2013).
- [62] A. Ibarra, A. S. Lamperstorfer, and J. Silk, (2013), arXiv:1309.2570 [hep-ph].

- [63] S. Desai *et al.* (Super-Kamiokande Collaboration), *Phys.Rev.* **D70**, 083523 (2004), arXiv:hep-ex/0404025 [hep-ex].
- [64] L. Covi, M. Grefe, A. Ibarra, and D. Tran, *JCAP* **1004**, 017 (2010), arXiv:0912.3521 [hep-ph].
- [65] 1089675, *Astrophys.J.* **750**, 3 (2012), arXiv:1202.4039 [astro-ph.HE].
- [66] M. Ackermann *et al.* (LAT Collaboration), *Phys.Rev.* **D86**, 022002 (2012), arXiv:1205.2739 [astro-ph.HE].
- [67] A. Abdo *et al.* (Fermi-LAT collaboration), *Phys.Rev.Lett.* **104**, 101101 (2010), arXiv:1002.3603 [astro-ph.HE].
- [68] T. Han, I. Lewis, and T. McElmurry, *JHEP* **1001**, 123 (2010), arXiv:0909.2666 [hep-ph].
- [69] G. F. Giudice, B. Gripaios, and R. Sundrum, *JHEP* **1108**, 055 (2011), arXiv:1105.3161 [hep-ph].
- [70] B. Grinstein, A. L. Kagan, J. Zupan, and M. Trott, *JHEP* **1110**, 072 (2011), arXiv:1108.4027 [hep-ph].
- [71] M. Bona *et al.* (UTfit Collaboration), *JHEP* **0803**, 049 (2008), arXiv:0707.0636 [hep-ph].
- [72] J. Charles, S. Descotes-Genon, Z. Ligeti, S. Monteil, M. Papucci, *et al.*, *Phys.Rev.* **D89**, 033016 (2014), arXiv:1309.2293 [hep-ph].
- [73] S. Chatrchyan *et al.* (CMS Collaboration), *Phys.Rev.Lett.* **110**, 141802 (2013), arXiv:1302.0531 [hep-ex].
- [74] C. Collaboration (CMS Collaboration), (2014).
- [75] ATLAS and C. Collaborations (ATLAS and CMS Collaborations), (2013).
- [76] J. Alwall, R. Frederix, S. Frixione, V. Hirschi, F. Maltoni, *et al.*, *JHEP* **1407**, 079 (2014), arXiv:1405.0301 [hep-ph].
- [77] A. Alloul, N. D. Christensen, C. Degrande, C. Duhr, and B. Fuks, *Comput.Phys.Commun.* **185**, 2250 (2014), arXiv:1310.1921 [hep-ph].
- [78] H. K. Dreiner, H. E. Haber, and S. P. Martin, *Phys.Rept.* **494**, 1 (2010), arXiv:0812.1594 [hep-ph].
- [79] M. D’Onofrio, K. Rummukainen, and A. Tranberg, *PoS LATTICE2012*, 055 (2012), arXiv:1212.3206.
- [80] J. A. Harvey and M. S. Turner, *Phys.Rev.* **D42**, 3344 (1990).

- [81] B. Feldstein and A. L. Fitzpatrick, JCAP **1009**, 005 (2010), arXiv:1003.5662 [hep-ph].
- [82] Y. Burnier, M. Laine, and M. Shaposhnikov, JCAP **0602**, 007 (2006), arXiv:hep-ph/0511246 [hep-ph].